JOURNAL OF COMPUTATIONAL PHYSICS 11, 360–399 (1973)

Numerical Simulation of Relativistic Electrons Confined in an Axisymmetric Mirror Field*

M. BRETTSCHNEIDER,† J. KILLEEN

University of California, Lawrence Livermore Laboratory, Livermore, California 94550 and Department of Applied Science, Davis, California 95616

AND

A. A. MIRIN

University of California, Lawrence Livermore Laboratory, Livermore, California 94550

Received April 14, 1972

A time-dependent numerical model of the astron, with which injection and trapping can be studied in detail, has been developed. The effects due to the resistors and neutralization have been included. The model is axially symmetric. The *E*-layer electrons are simulated by many thousands of finite-size superparticles, which move in the r–z domain and have velocity components v_r, v_θ, and v_z. The model is relativistic and the electromagnetic fields are obtained by solving four wave equations — three for the vector potential and one for the scalar potential. The *E*-layer current and the current induced in the resistor wires are included in the above field equations. The computed self-fields are added to the external field to give the field configuration as a function of time. Results of multiple pulse injection are presented.

I. INTRODUCTION

In the astron controlled-fusion experiment, a beam of relativistic electrons is injected into an evacuated cylindrical region in which an externally applied magnetic field has been established. The cylindrical region is bounded by two concentric aluminium shells. The outer shell is 12 cm thick and its inner radius is 72 cm. The thin inner shell has a radius of 20 cm. The velocity of the injected electrons makes an angle of 85° with the axis of symmetry. In order to facilitate trapping, cylinders of resistor wires, azimuthally oriented, have been installed at a radius of 52 cm and at a radius of 30 cm. The electrons that are trapped form

* Work performed under the auspices of the U.S. Atomic Energy Commission.

† Present address: Department of Physics, University of Tel Aviv, Tel Aviv, Israel.

a cylindrical layer (shell) known as the E layer. The mean radius of the E layer is 40 cm; its length varies from 1 to 4 m, depending on the initial conditions. The aim is to confine a sufficient number of electrons in the E layer so that the self field of the E layer exceeds the applied field. The resulting field configuration contains a region that is minimum $|B|$ and has no loss cones.

The E layer consists of about 10^{15} electrons. It is, of course, impractical to follow each electron individually. Furthermore, we are not interested in the position and velocity of each electron; we are only interested in the electron density. Since the electron density in the E layer is about $10^8/\text{cm}^3$ it is logical to treat the E layer as an electron fluid. The electron density can then be obtained from the solution of the Vlasov equation. Neil and Heckrotte [1], Woods [2], and Brettschneider and Weiss [3] examined the process of E layer formation in one dimension. In their model the electric and magnetic fields are obtained from the solution of Poisson's equation for the scalar and vector potentials, respectively. Retardation effects are neglected. The electron distribution in the E layer is obtained by integrating the Vlasov equation. Neil and Heckrotte and Brettschneider and Weiss integrate the Vlasov equation by using a finite difference fixed mesh point scheme, whereas Woods uses a water bag model.

A two-dimensional model was constructed by J. Killeen [4, 5]. Killeen uses a fixed mesh point, finite difference scheme to integrate the Vlasov equation. Complete neutralization is assumed; so the electric field is set equal to zero. The magnetic field is obtained by solving the wave equation for the azimuthal component of the vector potential. This method of obtaining the field is to be preferred since it include retardation. In view of the high axial and radial velocities ($\sim 0.5\,c$) achieved by the electrons, it is difficult to justify the neglect of retardation effects.

An alternate approach, which we use here, is to approximate the E layer by a large number of particles and follow each particle individually. The electron density is, then, obtained from the particle density. The force on a particle is obtained from the total electromagnetic field, and its trajectory is determined from the solution of the relativistic equations of motion.

The number of particles used must be large enough to give an accurate statistical representation of the E layer and yet small enough to be practical. In practice, we use between 10^4 and 3×10^4 particles. The principal advantage of this method over the fluid method is that it requires considerably less computation time to solve a given problem, and is more accurate for injection problems.

The computation proceeds as follows: First the charge and current densities are determined from the known initial positions and initial velocities of the particles. These charge and current densities are then used to determine the vector and scalar potentials by solving the respective wave equations. The new values of the vector and scalar potentials are used to calculate the force on each particle. These forces are used to move each particle in accordance with the relativistic

equations of motion. The above process is then repeated with the newly calculated positions and velocities.

The astron geometry is axisymmetric, and it is experimentally observed that the E layer, during most of its life, is also essentially axially symmetric. We therefore feel that the assumption of axial symmetry is a reasonable one to make.

In Section II the mathematical model is presented. The field equations, boundary conditions, and equations of motion are discussed in detail. Features which are specific to the Astron are introduced in Section III. The difference approximations are described in Section IV, and an energy check is described in Section V. In Section VI we discuss the computational results of a typical problem where five consecutive pulses are injected. Particular attention is given to the graphical output of the code.

II. Mathematical Model

A. *Field Equations*

If we employ the ralations

$$\mathbf{B} = \nabla \times \mathbf{A}, \qquad \mathbf{E} = -\nabla\phi - (1/c)(\partial A/\partial t), \qquad \nabla \cdot \mathbf{A} + (1/c)(\partial\phi/\partial t) = 0, \tag{1}$$

with Maxwell's equations, we obtain the following wave equations:

$$\nabla^2\mathbf{A} - (1/c^2)(\partial^2\mathbf{A}/\partial t^2) = -(4\pi/c)(\mathbf{j} + \mathbf{j}_{\text{res}}), \tag{2}$$

$$\nabla^2\phi - (1/c^2)(\partial^2\phi/\partial t^2) = -4\pi\rho, \tag{3}$$

where $\mathbf{A}$ and ϕ are the vector and scalar potentials; j, j_{res}, and ρ are the E-layer current density, resistor current density, and the charge density, respectively.

Assuming axial symmetry, Eqs. (2) and (3) become, in cylindrical coordinates,

$$\frac{\partial}{\partial r}\left[\frac{1}{r}\frac{\partial}{\partial r}(rA_r)\right] + \frac{\partial^2 A_r}{\partial z^2} - \frac{1}{c^2}\frac{\partial^2 A_r}{\partial t^2} = -\frac{4\pi j_r}{c}, \tag{4}$$

$$\frac{\partial}{\partial r}\left[\frac{1}{r}\frac{\partial}{\partial r}(rA_\theta)\right] + \frac{\partial^2 A_\theta}{\partial z^2} - \frac{1}{c^2}\frac{\partial^2 A_\theta}{\partial t^2} = -\frac{4\pi}{c}(j_\theta + j_{\theta\text{res}}), \tag{5}$$

$$\frac{1}{r}\frac{\partial}{\partial r}\left(r\frac{\partial A_z}{\partial r}\right) + \frac{\partial^2 A_z}{\partial z^2} - \frac{1}{c^2}\frac{\partial^2 A_z}{\partial t^2} = -\frac{4\pi j_z}{c}, \tag{6}$$

$$\frac{1}{r}\frac{\partial}{\partial r}\left(r\frac{\partial\phi}{\partial r}\right) + \frac{\partial^2\phi}{\partial z^2} - \frac{1}{c^2}\frac{\partial^2\phi}{\partial t^2} = -4\pi\rho. \tag{7}$$

B. *Boundary Conditions*

The domain of the model consists of two concentric grounded cylinders as shown in Fig. 1. The walls of the cylinders are assumed to be perfect conductors. This assumption is legitimate because of the short time scales. The boundary conditions at a perfect conductor are

$$B_{\perp} = 0, \qquad E_{\parallel} = 0. \tag{8}$$

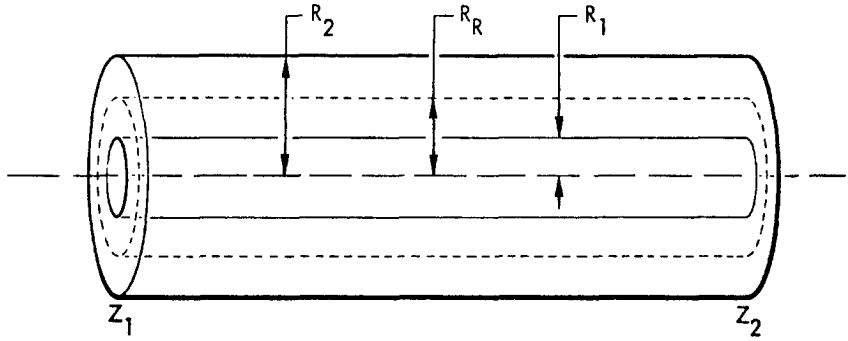

FIG. 1. Domain of the model: R_1 is the radius of the cantilever, R_R is the radius of the resistors, and R_2 is the inner radius of the outer wall.

These conditions are satisfied by

$$A_{\theta \mathrm{int}}(r, z) = 0 \text{ at all boundaries,} \tag{9}$$

$$\phi(r, z) = 0 \text{ at all boundaries and outside resistor layer,} \tag{10}$$

$$A_z(r, z) = 0 \text{ at } r = r_1, r_2, \text{ for all } z, \tag{11}$$

$$A_r(r, z) = 0 \text{ at } z = z_1, z_2, \text{ for all } r, \tag{12}$$

where $A_{\theta \mathrm{int}}$ is that part of A_θ which is generated by internal sources, i.e., currents in the E layer and in the resistors. The rest of A_θ, henceforth designated $A_{\theta \mathrm{coil}}$, is generated by current in the external coils. These currents are dc. Hence, the $A_{\theta \mathrm{coil}}$ has ample time to diffuse through the walls. The remaining boundary conditions are obtained from the gauge condition

$$\nabla \cdot \mathbf{A} + (1/c)(\partial \phi / \partial t) = 0. \tag{13}$$

They are

$$\partial / \partial r[r A_r(r, z)] \,|_{r=r_1, r_2} = 0 \qquad \text{for all } z, \tag{14}$$

and

$$\partial / \partial z[A_z(r, z)] \,|_{z=z_1, z_2} = 0 \qquad \text{for all } r. \tag{15}$$

C. *Superparticle Model*

The superparticles in this model are composed of a large number of electrons uniformly distributed throughout their volume. The shape of each superparticle is that of a ring of rectangular cross section.

The velocity of a superparticle has three components v_r, v_θ, and v_z. Since the superparticle is ring shaped, v_r refers to the speed with which it is expanding (contracting) and v_θ to the speed with which it rotates about the axis. v_z is the usual axial component of velocity.

The charge density ρ of a superparticle is given by

$$\rho = n_e(e/2\pi r\Delta r\Delta z), \tag{16}$$

where n_e is the number of electrons per superparticle, e the electronic charge, r the radius of the superparticle, Δr its radial thickness, and Δz its axial thickness.

The three components of the current density of a superparticle are given by

$$J_r = n_e(ev_r/2\pi r\Delta r\Delta z), \tag{17}$$

$$J_\theta = n_e(ev_\theta/2\pi r\Delta r\Delta z), \tag{18}$$

$$J_z = n_e(ev_z/2\pi r\Delta r\Delta z). \tag{19}$$

The field equations are solved in a domain that is subdivided by a finite difference mesh. The extent of this domain is given by

$$R_1 \leqslant r_j \leqslant R_2\,,\ -Z_1 \leqslant z_i \leqslant Z_2\,,\ J_1 \leqslant j \leqslant J_2\,,\ -I_1 \leqslant i \leqslant I_2\,,$$

where $r_j = j\Delta r$, $z_i = i\Delta z$, $R_1 = J_1\Delta r$, $R_2 = J_2\,\Delta r$, $Z_1 = I_1\Delta z$, and $Z_2 = I_2\Delta z$.

The charge and current densities must be known on the mesh points. The equations of motion yield the positions of the centers of the superparticles. These positions, usually, do not coincide with any mesh point. Therefore, some method must be devised whereby we can obtain the charge and current densities at the mesh points from the known positions and velocities of the superparticles. In the method that we use, the charge and current of a superparticle is shared among each of the four neighboring grid points in accordance with the standard area-weighting procedure. A simple way of visualizing this procedure is shown in Fig. 2 (we assume the charge to be uniformly distributed over the shaded region). Let the center of the particle be located in the zone (i, j) and let its coordinates be (z, r). The regions of the particle that are assigned to the neighboring grid points are denoted by

A_1, A_2, A_3, and A_4. A_1 is allocated to (i, j), A_2 to $(i + 1, j)$, A_3 to $(i, j + 1)$, and A_4 to $(i + 1, j + 1)$. The values of the A's are given by

$$A_1 = [(i + 1)\Delta z - z][(j + 1)\Delta r - r],$$
$$A_2 = (z - i\Delta z)[(j + 1)\Delta r - r],$$
$$A_3 = [(i + 1)\Delta z - z](r - j\Delta r),$$
$$A_4 = (z - i\Delta z)(r - j\Delta r).$$

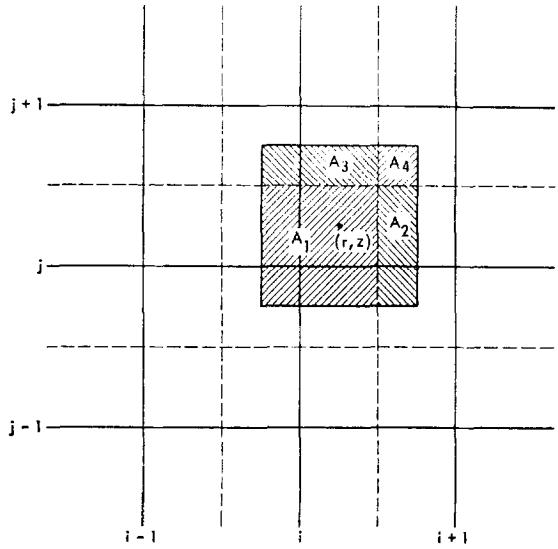

FIG. 2. Area weighting scheme for a superparticle.

To obtain the current and charge densities at a mesh point, the contributions from all the superparticles to that mesh point are summed.

D. *Equations of Motion*

We assume that the canonical angular momentum is a constant of the motion

$$m_0\gamma r^2\dot{\theta} + (e/c)\, rA_\theta = P_\theta = \text{const.} \tag{20}$$

It is convenient to introduce the function

$$\psi = (\gamma/c)\, r^2\dot{\theta}, \tag{21}$$

so that

$$\psi = P_\theta/m_0c - (e/m_0c^2)\, rA_\theta \tag{22}$$

and since we are assuming that all the particles have the same P_θ we can use ψ in place of A_θ. The rationale for introducing ψ is that it obviates the necessity of calculating v_θ, as will be apparent shortly.

We now introduce the dimensionless velocity $\mathbf{u}$ defined by

$$\mathbf{u} = (\gamma/c)\mathbf{v}, \tag{23}$$

where

$$\gamma = (1 - \underline{v}^2/c^2)^{-1/2}.$$

Substituting Eq. (23) into the expression for γ we get

$$\gamma = (1 + u_r^2 + u_\theta^2 + u_z^2)^{1/2}. \tag{24}$$

From Eq. (21) we have $\psi = ru_\theta$; hence

$$\gamma = (1 + u_r^2 + u_z^2 + (\psi^2/r^2))^{1/2}. \tag{25}$$

If we differentiate Eq. (23) with respect to time and rearrange the terms, we get

$$\begin{aligned} \ddot{r} &= (c/\gamma)\,\dot{u}_r - (c/\gamma^2)\,\dot{\gamma}u_r\,, \\ \ddot{z} &= (c/\gamma)\,\dot{u}_z - (c/\gamma^2)\,\dot{\gamma}u_z\,. \end{aligned} \tag{26}$$

Assuming axial symmetry, we have the following equations of motion:

$$m_0(\gamma\ddot{r} + \dot{\gamma}\dot{r} - \gamma r\dot{\theta}^2) = -e\frac{\partial\phi}{\partial r} - \frac{e}{c}\frac{\partial A_r}{\partial t} + \frac{e}{c}\left[r\dot{\theta}\,\frac{1}{r}\frac{\partial}{\partial r}(rA_\theta) - \dot{z}\left(\frac{\partial A_r}{\partial z} - \frac{\partial A_z}{\partial r}\right)\right], \tag{27}$$

$$m_0(\gamma\ddot{z} + \dot{\gamma}\dot{z}) = -e\frac{\partial\phi}{\partial z} - \frac{e}{c}\frac{\partial A_z}{\partial t} + \frac{e}{c}\left[\dot{r}\left(\frac{\partial A_r}{\partial z} - \frac{\partial A_z}{\partial r}\right) + r\dot{\theta}\,\frac{\partial A_\theta}{\partial z}\right]. \tag{28}$$

Substitution of Eqs. (23) and (26) into Eqs. (27) and (28) yields for the radial equation of motion

$$\frac{du_r}{dt} = -\frac{c}{\gamma}\frac{\partial}{\partial r}\left(\frac{\psi^2}{2r^2}\right) - \frac{e}{m_0 c}\frac{\partial\phi}{\partial r} - \frac{e}{m_0 c^2}\left[\frac{\partial A_r}{\partial t} - \frac{c}{\gamma}u_z\left(\frac{\partial A_r}{\partial z} - \frac{\partial A_z}{\partial r}\right)\right]. \tag{29}$$

Similarly the axial equation of motion becomes

$$\frac{du_z}{dt} = -\frac{c}{\gamma}\frac{\partial}{\partial z}\left(\frac{\psi^2}{2r^2}\right) - \frac{e}{m_0 c}\frac{\partial\phi}{\partial z} - \frac{e}{m_0 c^2}\left[\frac{\partial A_z}{\partial t} + \frac{c}{\gamma}u_r\left(\frac{\partial A_r}{\partial z} - \frac{\partial A_z}{\partial r}\right)\right]. \tag{30}$$

E. *Dimensionless Formulation*

We now introduce the dimensionless function $\bar{\mu}$ defined by

$$\bar{\mu} = \frac{\psi}{(P_\theta/m_0 c)} . \tag{31}$$

In order to evaluate the denominator we consider an equilibrium orbit in a uniform vacuum field. For such a field it is true that

$$A_\theta(r, z) = \tfrac{1}{2} B_0 r, \tag{32}$$

where B_0 is that axial component of the field. From the radial equation of motion we have

$$m_0 \gamma r_0 \dot{\theta}^2 = -(e/c)\, r_0 \dot{\theta} B_0 , \tag{33}$$

where r_0 is the radius of the orbit. Hence

$$P_\theta = -(e/c)\, B_0 r_0^2 + 1/2(e/c)\, B_0 r_0^2 = -1/2(e/c)\, B_0 r_0^2 \tag{34}$$

and

$$\bar{\mu} = -(2m_0 c^2/eB_0 r_0^2)\psi. \tag{35}$$

We now introduce the rest of our dimensionless variables

$$R = r/r_0 , \qquad Z = z/r_0 , \qquad \tau = ct/r_0 \tag{36}$$

$$\bar{a}_\theta = A_\theta/B_0 r_0 , \quad a_r = 2rA_r/B_0 r_0^2, \quad a_z = 2A_z/B_0 r_0 , \quad \chi = (e/m_0 c^2)\phi \tag{37}$$

$$\bar{b}_r = B_r/B_0 , \qquad \bar{b}_z = B_z/B_0 , \qquad b_\theta = B_\theta/B_0$$

and (38)

$$e_r = E_r/B_0 , \qquad e_z = E_z/B_0 , \qquad e_\theta = E_\theta/B_0 .$$

From these definitions and Eqs. (1), (22), and (39)

$$\bar{\mu} = 1 + 2R\bar{a}_\theta \tag{39}$$

$$\begin{gathered} \bar{b}_r = -(1/2R)(\partial\bar{\mu}/\partial Z), \qquad \bar{b}_z = (1/2R)(\partial\bar{\mu}/\partial R), \\ b_\theta = (1/2R)(\partial a_r/\partial Z) - (1/2)(\partial a_z/\partial R), \end{gathered} \tag{40}$$

$$\begin{gathered} e_r = -(e/B_0 r_0 r_e)(\partial\chi/\partial R) - (1/2R)(\partial a_r/\partial\tau), \\ e_z = -(e/B_0 r_0 r_e)(\partial\chi/\partial Z) - (1/2)(\partial a_z/\partial\tau), \qquad e_\theta = -(1/2R)(\partial\bar{\mu}/\partial\tau), \end{gathered} \tag{41}$$

where e_r, e_z, and e_θ are the dimensionless components of the electric field and $r_e = e^2/m_0c^2$ is the classical radius of the electron.

It is convenient to let

$$\bar{\mu} = \mu_c + \mu, \tag{42}$$

where μ_c represents the vacuum field and μ represents the field of the E layer. The function μ_c satisfies the equation

$$\partial^2\mu_c/\partial\tau^2 - \partial^2\mu_c/\partial Z^2 - R(\partial/\partial R)\,((1/R)(\partial\mu_c/\partial R)) = 0. \tag{43}$$

We introduce the parameter

$$C_1 = -eB_0r_0/2m_0c^2 = -(2.93 \times 10^{-4})\,B_0r_0 \tag{44}$$

and define the function $P(R, Z, \tau)$ by

$$P = (1/2)\,C_1^2(\bar{\mu}^2/R^2). \tag{45}$$

Using Eqs. (35)–(37) and (44) we can write the equations of motion (29) and (30) in dimensionless form as follows:

$$\frac{du_r}{d\tau} = -\frac{1}{\gamma}\frac{\partial P}{\partial R} - \frac{\partial\chi}{\partial R} + \frac{C_1}{R}\frac{\partial a_r}{\partial\tau} - \frac{C_1}{\gamma}u_z\left(\frac{1}{R}\frac{\partial a_r}{\partial Z} - \frac{\partial a_z}{\partial R}\right) = \frac{-F_r}{\gamma}, \tag{46}$$

$$\frac{du_z}{d\tau} = -\frac{1}{\gamma}\frac{\partial P}{\partial Z} - \frac{\partial\chi}{\partial Z} + C_1\frac{\partial a_z}{\partial\tau} + \frac{C_1}{\gamma}u_r\left(\frac{1}{R}\frac{\partial a_r}{\partial Z} - \frac{\partial a_z}{\partial R}\right) = \frac{-F_z}{\gamma}. \tag{47}$$

We now introduce the dimensionless quantities I_θ, I_r, I_Z, and I_ρ corresponding to the dimensionless current and charge densities

$$I_\theta = \frac{8\pi r_0R}{cB_0}\sum J_\theta = -\frac{2n_er_e}{\Delta R\,\Delta Z\,r_0}\sum\frac{\bar{\mu}}{R\gamma}, \tag{48}$$

$$I_r = \frac{8\pi r_0R}{cB_0}\sum J_r = \frac{4n_ee}{B_0\,\Delta R\,\Delta Z\,r_0^2}\sum\frac{u_r}{\gamma}, \tag{49}$$

$$I_Z = \frac{8\pi r_0}{cB_0}\sum J_Z = \frac{4n_ee}{B_0\,\Delta R\,\Delta Z\,r_0^2}\sum\frac{u_z}{R\gamma}, \tag{50}$$

$$I_\rho = \frac{4\pi er_0^2}{m_0c^2}\sum\rho = \frac{2n_er_e}{\Delta R\,\Delta Z\,r_0}\sum\frac{1}{R}, \tag{51}$$

where we used Eqs. (21), (23), (35), and (36) to write the right-hand sides of Eqs. (16)–(19) in terms of dimensionless quantities. The symbol $\sum$ in the above equations represents a sum over the contributions of all the particles in that region of space, as explained in Section I-B.

Finally, using Eqs. (36) and (37), we can write the wave equations (4)–(7) in dimensionless form:

$$R\frac{\partial}{\partial R}\left(\frac{1}{R}\frac{\partial a_r}{\partial R}\right)+\frac{\partial^2 a_r}{\partial Z^2}-\frac{\partial^2 a_r}{\partial \tau^2}=-I_r\,, \tag{52}$$

$$R\frac{\partial}{\partial R}\left(\frac{1}{R}\frac{\partial \mu}{\partial R}\right)+\frac{\partial^2 \mu}{\partial Z^2}-\frac{\partial^2 \mu}{\partial \tau^2}=-(I_\theta+I_{\theta\mathrm{res}}), \tag{53}$$

$$\frac{1}{R}\frac{\partial}{\partial R}\left(R\frac{\partial a_z}{\partial R}\right)+\frac{\partial^2 a_z}{\partial Z^2}-\frac{\partial^2 a_z}{\partial \tau^2}=-I_Z\,, \tag{54}$$

$$\frac{1}{R}\frac{\partial \chi}{\partial R}\left(R\frac{\partial \chi}{\partial R}\right)+\frac{\partial^2 \chi}{\partial Z^2}-\frac{\partial^2 \chi}{\partial \tau^2}=-I_\rho\,. \tag{55}$$

The boundary conditions in dimensionless form are

$$\mu(R, Z)=0 \quad \text{at all boundaries,} \tag{56}$$

$$\chi(R, Z)=0 \quad \text{at all boundaries and at the resistor layer,} \tag{57}$$

$$a_z(R, Z)=0 \quad \text{at } R=R_1\,,\ R_2 \quad \text{for all } Z, \tag{58}$$

$$a_r(R, Z)=0 \quad \text{at } Z=-Z_1\,,\ Z_2 \quad \text{for all } R, \tag{59}$$

$$(\partial a_r/\partial R)\,(R, Z)=0 \quad \text{at } R=R_1\,,\ R_2 \quad \text{for all } Z, \tag{60}$$

$$(\partial/\partial Z)a_z\,(R, Z)=0 \quad \text{at } Z=-Z_1\,,\ Z_2 \quad \text{for all } R. \tag{61}$$

III. Special Features of the Astron Model

A. *Current in the Resistors*

The function of the resistors is to extract energy from the E-layer electrons. The resistors consist of a large number of very fine (1.5 mil) wires. They are wound on a cylindrical frame of fixed radius such that the current in them flows in the θ direction only. It is convenient to replace the individual resistor wires with a resistor sheet.

The current density in the resistors is given by $j_{\theta\mathrm{res}}=\sigma_\theta E_\theta$, where σ_θ is the conductivity of the resistor sheet and E_θ the θ component of the electric field at the resistors. E_θ is calculated from $E_\theta=-(1/c)(\partial A_\theta/\partial t)$, where A_θ is the θ com-

ponent of the vector potential. The current density j_θ, given above, cannot be used in the field calculation since no allowance has been made for the fact that the radial thickness of a zone Δr is much greater than the radial thickness of the resistor sheet. The proper current density is given by

$$\begin{aligned} j_{\theta\text{res}} &= -(\sigma_\theta \delta_\theta/\Delta r)(1/c)(\partial A_\theta/\partial t) \qquad \text{at} \quad r = r_{\text{res}}, \\ j_{\theta\text{res}} &= 0 \qquad\qquad\qquad\qquad\qquad\quad \text{at} \quad r \neq r_{\text{res}}, \end{aligned} \tag{62}$$

where δ_θ is the radial thickness of the resistor sheet, and r_{res} is the radius of the resistor layer. In the astron experiment and in the model there are two resistor layers—an inner layer at a radius of 30 cm and an outer layer at a radius between 50 and 60 cm. The resistor radius can be varied as a function of z, and the resistor configuration is one of the variable features of the experiment and the model.

B. *Injection Scheme*

The number of superparticles injected per time step is given by $N_T \Delta\tau/\tau_{\text{PL}}$, where N_T is the total number of particles that will be used per pulse, $\Delta\tau$ is the time step, and τ_{PL} is the pulse length.

A superparticle is a ring of circulating charge. The current of this ring is given by $n_e e/\tau_B$, where e is the electronic charge, n_e is the number of electrons per superparticle, and τ_B is the cyclotron period. Hence the current injected per time step is given by

$$I_{\Delta t} = (n_e e/\tau_B) \cdot (N_T \Delta\tau/\tau_{\text{PL}}).$$

If a current I is injected into astron, we have, at the end of one cyclotron period, a current I circulating in the machine. Therefore the current that has to be injected per time step is $(\Delta\tau/\tau_B)I$. Hence

$$n_e = I\tau_{\text{PL}}/eN_T. \tag{63}$$

Each time step, during injection of a pulse, the required number of superparticles are injected at a set of Z positions in the neighborhood of the injector location. We can inject the particle into a region where the radial force on it is small in order to minimize early radial fluctuations. For a given Z we calculate R such that F_r in Eq. (46) is zero, where R is in the neighborhood of the injector.

C. *Neutralization Scheme*

To see how we can incorporate the neutralization phenomenon into the model, we must look at the process in detail. We will do so by looking at one region in

space and see how neutralization proceeds with time. Consider a small region of neutral gas into which a bunch of electrons has entered. The electrons remain in this region for a time δt. By the time they leave, they will have undergone n_i ionizing collisions. Since the incident electron bunch has a high electric field associated with it, the cold electrons that are freed by the ionizing collisions are accelerated out of the region. When the electron bunch leaves, the region contains n_i positive ions. Now let another bunch of electrons with the same density and pulse length enter this region. It too undergoes ionizing collisions and the electrons liberated by these collisions are again accelerated out of the region, only not as fast as the first ones since the electric field of the second bunch is slightly masked by the field of the residual n_i positive ions. If we now imagine similar bunches entering the region in succession, the number of positive ions in the region will build up until the number of ions equals the number of electrons in the incident beam.

Each region in space must be given a certain amount of positive charge. This amount depends on how much cumulative time electrons have spent in that region. Therefore, the net amount of charge in a given region at a given time is the number of electrons in the region minus the number of positive ions in the region.

As explained earlier, the r, z configuration space in the model is divided into a finite-difference grid. The smallest region in the model is that of a zone. Each zone is, therefore, assigned a number of positive ions commensurate with the amount of neutralization that occurred in that zone.

Let us consider a beam of M electrons circulating in one zone. The number of ionizing collisions made by this beam of electrons in a distance $c\delta t$ is given by $n_i = NQMc\delta t$, where N is the number of gas atoms per cm^3, Q is the ionization cross section, and M is the number of beam electrons, and c is the velocity of light. Note that the ratio $n_i/M = NQc\delta t$ is independent of electron density. This ratio can also be interpreted as the fraction of the beam neutralized in time δt. Replacing electrons with superparticles, we can say that $NQc\delta t$ is the fraction of the superparticle charge that is neutralized in time δt. If we assume that the background gas is ideal, the pressure P is given by $P = NKT$. Letting $T = 300°$K, writing the pressure in microns and δt in nanoseconds, and using $Q = 2.35 \times 10^{-14}$ cm^2, we have $NQc\delta t = 2.5 \times 10^{-4} P\delta t$.

We now summarize the process. Let M superparticles enter a zone. After one time step, $\Delta\tau$, they contribute $n_i = 2.5 \times 10^{-4} MP\Delta t$ positive ions to that space.

At present we do not allow a region to have a net positive charge. If the number of positive ions exceeds the number of electrons the net charge in the region is assumed to be zero. The rationale for this is that a region which has a net positive charge very quickly sucks in enough cold electrons from the background to neutralize that charge.

When we use the neutralization option, we are in effect creating a plasma. This plasma can and does carry currents. These currents are neglected. It is true that in some circumstances the axial plasma currents may be comparable in magnitude to the axial E layer currents, resulting in serious errors in the calculation of A_z. These circumstances arise later in time after a significant amount of neutralization has taken place. However, early in time when the particles are being injected and are traveling down the ramp in an essentially unneutralized region, the axial currents due to the particles are much greater than the axial plasma currents. This is due to the large axial velocities ($\sim 0.5\,c$) which the particles attain. The location of the crossover point depends on the individual case.

While it is true that there are radial plasma currents as well, it is unlikely that they are comparable to the radial E-layer current since the plasma electrons are cold and would therefore have to diffuse across the field lines.

The present neutralization scheme causes an error in the energy check since, by turning off a part of the negative charge, the energy in the electric field is diminished. This energy loss is not included in the energy check.

IV. Difference Equations

The field equations are solved on a finite difference mesh. The mesh spacing is given by $\Delta R = h$, $\Delta Z = mh$. The position on the mesh is given by $R_j = jh$, $Z_i = imh$, where $-I_1 \leqslant i \leqslant I_2$ and $J_1 \leqslant j \leqslant J_2$. A given time is denoted by an integral number of time steps, i.e., $\tau_n = n\Delta\tau$, where $n = 0, 1, 2, \ldots$. We now introduce the notation $\mu_{ij}^n = \mu(R_j, Z_i, \tau_n)$, etc.

The difference approximation that we use in solving the field equations is called the Alternating Direction Implicit (ADI) method. In the first half-time step the equation is implicit in the R direction and explicit in the Z direction, and in the second half time step the equation is explicit in R and implicit in Z.

The difference equation corresponding to Eq. (53) for the first half-time step is

$$\frac{\mu_{ij}^{n+1/2} - 2\mu_{ij}^{n} + \mu_{ij}^{n-1/2}}{(\Delta\tau/2)^2} = \frac{2j}{h^2}\left[\frac{\mu_{i,j+1}^{n+1/2} - \mu_{ij}^{n+1/2}}{2j+1} - \frac{\mu_{ij}^{n+1/2} - \mu_{i,j-1}^{n+1/2}}{2j-1}\right] + \frac{\mu_{i+1,j}^{n} - 2\mu_{ij}^{n} + \mu_{i-1,j}^{n}}{m^2h^2} + c_2\frac{\mu_{ij}^{n+1/2} - \mu_{ij}^{n-1/2}}{\Delta\tau} + I_{\theta ij}^{n}, \tag{64a}$$

and the equation for the second half-time step is

$$\frac{\mu_{ij}^{n+1} - 2\mu_{ij}^{n+1/2} + \mu_{ij}^{n}}{(\Delta\tau/2)^2} = \frac{\mu_{i+1,j}^{n+1} - 2\mu_{ij}^{n+1} \quad \mu_{i-1,j}^{n+1}}{m^2h^2} + I_{\theta ij}^{n+1/2}$$

$$+ \frac{2j}{h^2}\left[\frac{\mu_{i,j+1}^{n+1/2} - \mu_{ij}^{n+1/2}}{2j+1} - \frac{\mu_{ij}^{n+1/2} - \mu_{i,j-1}^{n+1/2}}{2j-1}\right]$$

$$+ c_2 \frac{\mu_{ij}^{n+1} - \mu_{ij}^{n}}{\Delta\tau}, \tag{64b}$$

where $c_2 = -4\pi/\mathrm{ch}\ \sigma_\theta\delta_\theta$ for $R = R_{\mathrm{res}}$ and $c_2 = 0$ for $R \neq R_{\mathrm{res}}$. A similar pair of difference equations is used to approximate Eq. (52). The difference equation corresponding to Eq. (55) for the first half-time step is

$$\frac{\chi_{ij}^{n+1/2} - 2\chi_{ij}^{n} + \chi_{ij}^{n-1/2}}{(\Delta\tau/2)^2} = \frac{1}{2jh^2}[(2j+1)(\chi_{i,j+1}^{n+1/2} - \chi_{ij}^{n+1/2}) - (2j-1)(\chi_{ij}^{n+1/2} - \chi_{i,j-1}^{n+1/2})]$$

$$+ \frac{\chi_{i+1,j}^{n} - 2\chi_{ij}^{n} + \chi_{i-1,j}^{n}}{m^2h^2} + I_{\rho ij}^{n}, \tag{65a}$$

and the equation for the second half-time step is

$$\frac{\chi_{ij}^{n+1} - 2\chi_{ij}^{n+1/2} + \chi_{ij}^{n}}{(\Delta\tau/2)^2} = \frac{\chi_{i+1,j}^{n+1} - 2\chi_{ij}^{n+1} + \chi_{i-1,j}^{n+1}}{m^2h^2}$$

$$+ \frac{1}{2jh^2}[(2j+1)(\chi_{i,j+1}^{n+1/2} - \chi_{ij}^{n+1/2})$$

$$- (2j-1)(\chi_{ij}^{n+1/2} - \chi_{i,j-1}^{n+1/2})] + I_{\rho ij}^{n+1/2}. \tag{65b}$$

A similar pair of difference equations is used to approximate Eq. (54). The method of solving the four pairs of implicit difference equations is the standard algorithm for solving linear tridiagonal systems and is discussed in Ref. [4].

An alternate method of solving the field equations is the following explicit scheme, shown only for the μ equation for the first half-time step:

$$\frac{\mu_{ij}^{n+1/2} - 2\mu_{ij}^{n} + \mu_{ij}^{n-1/2}}{(\Delta\tau/2)^2} = \frac{\mu_{i+1,j}^{n} - 2\mu_{ij}^{n} + \mu_{i-1,j}^{n}}{m^2h^2} + I_{\theta ij}^{n}$$

$$+ \frac{2j}{h^2}\left(\frac{\mu_{i,j+1}^{n} - \mu_{ij}^{n}}{2j+1} - \frac{\mu_{ij}^{n} - \mu_{i,j-1}^{n}}{2j-1}\right)$$

$$+ c_2(\mu_{ij}^{n+1/2} \quad \mu_{ij}^{n-1/2})/\Delta\tau.$$

We compared the two methods by running a sample problem for 1000 cycles using the explicit scheme. We found that the results agree to within 5 % or better in the field quantities, and within 1 % in the particle distribution functions.

The principal difference between the two schemes lies in the fact that the ADI has inherent damping, while the explicit scheme does not. This damping is not altogether unwelcome. For instance, it tends to decrease the errors introduced by our neutralization scheme. These errors arise from the discontinuous reduction of the charge density caused by the neutralization process. These discontinuous charge reductions create spurious waves which are damped by the ADI scheme.

Furthermore, we have found that the Lorentz condition

$$\nabla \cdot \mathbf{A} + (1/c)\,(\partial\phi/\partial t) = 0$$

is more closely approximated by the ADI scheme. This can be attributed to the damping characteristics of the scheme since the source of the error is primarily in the short wavelengths.

The effect of not satisfying the Lorentz condition is to create false charges. This can be seen by writing the wave equation without assuming that the Lorentz condition is satisfied. In this case, the wave equations becomes

$$\nabla \cdot \mathbf{E} - 4\pi\rho = -\left(\nabla^2\phi - \frac{1}{c^2}\frac{\partial^2\phi}{\partial\tau^2} + 4\pi\rho\right) - \frac{1}{c}\frac{\partial}{\partial t}\left(\nabla \cdot \mathbf{A} + \frac{1}{c}\frac{\partial\phi}{\partial t}\right).$$

We evaluated the quantity $-(1/c)(\partial/\partial t)[\nabla \cdot \mathbf{A} + (1/c)(\partial\phi/\partial t)]$ in two test cases. In one test case we used the explicit scheme, and in the other we used the implicit scheme. In the test case, we injected 1000 particles 0.02 cm from the left end wall into a region with 50 axial zones. Each particle had a current of 1 A. Furthermore, each particle was given a slightly different axial velocity so that at the end of 500 cycles the particles would be uniformly spread over the central 25 axial zones. We compared the results at cycles 600 and 1000. The total real charge ($4\pi\rho$) was, in dimensionless units, 5.77×10^{-1}, and remained constant during the run. When the fields were calculated by using the explicit scheme, the total false $\{-(1/c)(\partial/\partial t)[\nabla \cdot \mathbf{A} + (1/c)(\partial\phi/\partial t)]\}$ charge created was, again in dimensionless units, -1.9×10^{-2} at cycle 600 and 2.75×10^{-3} at cycle 1000. Whereas, when we used the implicit scheme, the false charge at cycle 600 was -9.35×10^{-5} and -1.8×10^{-6} at 1000.

The equations of motion (46) and (47) are approximated by the centered difference equations

$$(u_r^{n+1} - u_r^{n-1})/2\Delta\tau = -F_r{}^n/\gamma^n, \tag{66}$$

$$(u_z^{n+1} - u_z^{n-1})/2\Delta\tau = -F_z{}^n/\gamma^n, \tag{67}$$

where

$$\gamma^n = \{1 + (u_r{}^n)^2 + (u_z{}^n)^2 + C_1{}^2[(\bar{\mu}^n)^2/R^2]\}^{1/2}.$$

The superparticle positions are then obtained from

$$(R^{n+1} - R^n)/\Delta\tau = (u_r^{n+1} + u_r^n)/2\gamma^n , \tag{68}$$

$$(Z^{n+1} - Z^n)/\Delta\tau = (u_z^{n+1} + u_z^n)/2\gamma^n, \tag{69}$$

where we have retained u_r^n, u_z^n in order to compute the above average. (It is unnecessary to evaluate γ at $\tau_{n+1/2}$ since γ changes slowly).[1]

All the above quantities u_z , u_r , γ, Z, R, F_z , F_r are evaluated at the particle centers. Since F_z and F_r are calculated from the fields which are given at the mesh points only, we use linear interpolation to get their values at the particle centers.

This scheme has two coupled solutions—one consists of velocities at even-numbered cycles and positions at odd-numbered cycles, the other consists of velocities at odd-numbered cycles and positions at even-numbered cycles. These solutions tend to grow apart so they must be synchronized periodically, usually every hundred time steps. The method for doing this is the following initialization procedure which is also used for obtaining starting values. We first obtain trial values from

$$\begin{aligned}
(u_r^* - u_r^n)/\Delta\tau &= -F_r^n/\gamma^n, \\
(u_z^* - u_z^n)/\Delta\tau &= -F_z^n/\gamma^n, \\
(R^* - R^n)/\Delta\tau &= (u_r^* + u_r^n)/2\gamma^n, \\
(Z^* - Z^n)/\Delta\tau &= (u_z^* + u_z^n)/2\gamma^n.
\end{aligned}$$

We then obtain new values at τ_{n+1} from

$$\begin{aligned}
(u_r^{n+1} - u_r^n)/\Delta\tau &= -(F_r^* + F_r^n)/2\gamma^n, \\
(u_z^{n+1} - u_z^n)/\Delta\tau &= -(F_z^* + F_z^n)/2\gamma^n, \\
(R^{n+1} - R^n)/\Delta\tau &= (u_r^{n+1} + u_r^n)/2\gamma^n, \\
(Z^{n+1} - Z^n)/\Delta\tau &= (u_z^{n+1} + u_z^n)/2\gamma^n.
\end{aligned}$$

In the above, F_r^* and F_z^* are based on u_r^*, u_z^*, R^*, Z^* and the fields at time n.[2]

[1] We have since found that it is necessary to evaluate γ at $\tau_{n+\frac{1}{2}}$, and we use an iterative procedure to do so.

[2] We have since changed the difference scheme and have employed an iterative procedure so as to eliminate the need for synchronization.

V. Conservation of Energy

During the calculation we independently monitor the number of particles and total energy present in the system. Particles can be lost at all of the physical boundaries in the r–z domain and we count the particles lost at each boundary for each pulse injected.

The total energy present in the system at a given time is the sum of the energy in the electromagnetic field and the kinetic energy of the particles. The energy in the field is

$$\frac{1}{8\pi}\int_0^{2\pi} d\theta \int_{-l}^{+l} dz \int_0^{r_{\max}} r\, dr[B^2 + E^2].$$

If we divide the above expression by the constant $r_0{}^3B_0{}^2/4$, we obtain the dimensionless quantity

$$\mathscr{E}_{\mathrm{EM}} = \int_{-Z_1}^{Z_2} dZ \int_{R_1}^{R_2} R\, dR[\bar{b}_r{}^2 + b_\theta{}^2 + \bar{b}_z{}^2 + e_r{}^2 + e_\theta{}^2 + e_z{}^2], \tag{70}$$

where we use the definitions of Eqs. (40) and (41).

The kinetic energy of a superparticle is $n_e\gamma_\nu m_0c^2$, where ν is the particle index; hence the total energy of all the particles is

$$T = \frac{4n_em_0c^2}{B_0{}^2r_0{}^3}\sum_{\nu=1}^{N}\gamma_\nu\,, \tag{71}$$

where we have divided by $r_0{}^3B_0{}^2/4$.

The amount of energy dissipated in one time step, in one axial zone Δz of the resistors is

$$\Delta t(2\pi r/\sigma_\theta\delta_\theta\,\Delta z)(\Delta z\,\Delta r)^2 j_{\theta\mathrm{res}}^2\,,$$

where $j_{\theta\mathrm{res}}$ is given by Eq. (62). We use the dimensionless current

$$\begin{aligned} I_{\theta\mathrm{res}} &= (8\pi/c)(r_0R/B_0)\, j_{\theta\mathrm{res}} \\ &= -(4\pi/c)(\sigma_\theta\delta_\theta/\Delta R)(\partial\mu/\partial\tau). \end{aligned} \tag{72}$$

If we sum over axial zones and use the dimensionless variables, we have

$$\mathscr{E}_{\Delta t} = \Delta\tau\sum_i \frac{c}{8\pi}\,\Delta Z(\Delta R)^2\,\frac{1}{\sigma_\theta\delta_\theta R}\,[(I_{\theta\mathrm{res}})_{ij}^n]^2, \tag{73}$$

where we have divided by $r_0{}^3B_0{}^2/4$. We then define the total energy dissipated in the

resistors up to time n by substituting Eq. (72) into Eq. (73) and summing the contributions of each time step,

$$\mathscr{E}^n_{\Delta t} = \frac{2\pi}{c} \sum_{m=1}^{n} \Delta\tau \sum_i \Delta Z \frac{\sigma_\theta \delta_\theta}{R_{\text{res}}} \left[\frac{\mu^m_{ij} - \mu^{m-1}_{ij}}{\Delta\tau} \right]^2. \tag{74}$$

When a particle hits the wall, the only energy lost is its kinetic-energy, because the image charge and image current cancel the field of the particle as it nears the wall. We denote this energy by

$$T_{\text{loss}} = \frac{4 n_e m_0 c^2}{B_0^2 r_0^3} \sum_{\nu=1}^{N_{\text{loss}}} \gamma_\nu ,$$

where N_{loss} is the number of particles lost. Therefore, the quantity

$$\mathscr{E}_{\text{EM}} + T + \mathscr{E}^n_{\Delta t} + T_{\text{loss}}$$

must be constant after injection has stopped. The quantity $\mathscr{E}^n_{\Delta t}$ is computed for both inner and outer resistor layers and the above expression includes their sum.

VI. Computational Results

In a typical astron run, a beam of relativistic electrons is injected into a region in which a solenoidal mirror field has been established. The beam current varies, depending on the experiment, from 100 to 800 A. Similarly, the pulse length varies from 100 to 300 nsec. The average electron energy is about 5.5 MeV. The background pressure varies from about 2 μ to about 50 μ. Generally, it is about 10 μ. The shape of the applied field depends on the experiment. When the object is to optimize trapping (as it usually is) the shape of the field near the injection point is that of a shallow mirror, whereas the field at the far end of the intended trapping region is a steep mirror.

In Ref. [6] we showed results for the injection and trapping of a pulse of 800 A of 200 nsec duration. We represented that pulse by 21 000 superparticles. When that pulse had settled down in time, we injected a second 800-A pulse of 100-nsec duration, which we represented by 10 500 superparticles.

In this paper we show the results of overlapping five consecutively injected pulses. Each succeeding pulse is injected after the previously injected particles have reached steady state. We use the same applied magnetic field as in the previous

case which is computed from a set of circular coils corresponding to an actual experimental configuration. The physical parameters for the problem are:

Injection current	800 A
Pulse length	100 nsec
Axial injection velocity	0.1 c
Radial injection velocity	0
Number of particles injected per pulse	4500
Number of pulses	5
Background pressure	10 μ
Magnetic field	Fig. 3
Resistance	7 Ω/square
Resistor radius	52 cm
Tank radius (inner)	72 cm
Injection radius	$\sim$ 40 cm
Injection energy	5.28 MeV

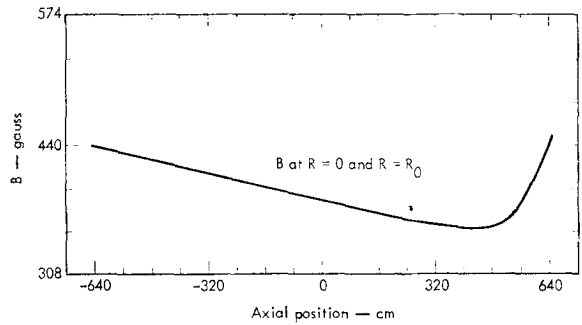

FIG. 3. Plot of B_z vs z at two radial positions, $R = 0$ and $R = 40$ cm at 0.132 nsec.

The mesh parameters were:

Number of axial zones	100
Number of radial zones	18
Axial space step Δz	13 cm
Radial space step Δr	4 cm
Time step (field equation)	0.067 nsec
Time step (particle equation of motion)	0.267 nsec
Total No. of particles injected	22 500

The particles were injected into the second zone from the left end boundary. Injection of the first pulse begins at $t = 0$ and ends at $t = 100$ nsec (Fig. 4). We see the characteristic dip in phase space (Fig. 4a). By $t = 148$ nsec, the leading edge of the first pulse has reached the end of the far mirror (Fig. 5). From Fig. 5c we see that a clump has formed on the trailing edge of the pulse. The reason for this is that the particles injected last have overtaken some of the particles injected earlier (Fig. 5a). By this time the injection region has been sufficiently ionized so that the magnetic attraction between the particles exceeds the electrostatic repulsion. Hence, the particles in the trailing edge see a net force drawing them toward the other particles. This force is greatest on the particles injected last since the only force that they see is from the right.

In marked contrast, the particles injected first are put into a region in which there has been no ionization at all. Between these particles, the electrostatic repelling force exceeds the magnetic attracting force. Hence, they are accelerated away from the other particles. When the leading particles reach the far mirror, those particles in the extreme leading edge acquire enough energy to climb the far mirror and leave the system. These are the only particles from the first pulse that are lost.

Figure 6 shows the state of the system at $t = 268$ nsec. We see that the particles in the dip move much more slowly than the other particles. All particles continue to bounce back and forth between the two mirrors, thermalizing in the process. By $t = 1300$ nsec, the system has almost reached steady state (Fig. 7a and 7g). The bottom of the well is located 10.8 m from the injection end. Figure 7i shows the radial variation of J_θ at the bottom of the well. There are 4461 particles in the system. These give 9517 circulating amperes. Figure 7j shows that the axial field at the bottom of the well is 10% weaker than the corresponding vacuum field.

Injection of the second pulse began at $t = 1300$ nsec. Figure 7 shows the second pulse coming in at the left end. Injection of this pulse ceased at $t = 1400$ nsec (Fig. 8). Comparison of Figs 4c and 8c shows that there is considerably more self-pinching in the second pulse. This is because the region through which the second pulse is moving has been partially ionized by the first pulse. A consequence of this greater self-pinching is the stronger coupling between the second pulse and the resistors. This is readily apparent when one compares the currents induced in the resistors by the respective pulses (Figs. 4d and 8d).

The second pulse reaches the end of the far mirror by $t = 1520$ nsec (Fig. 9). Figures 9a, c, and d clearly show that the second pulse has split into a number of distinct bunches. From Figs. 9a and e we also see that a number of particles from the second pulse have left the system by climbing the far mirror. This time, however, the accelerating force which provides these particles with sufficient energy to leave the system originates with the particles of the first pulse which attract the particles from the second pulse. The major loss of particles from the second pulse occurs at this time.

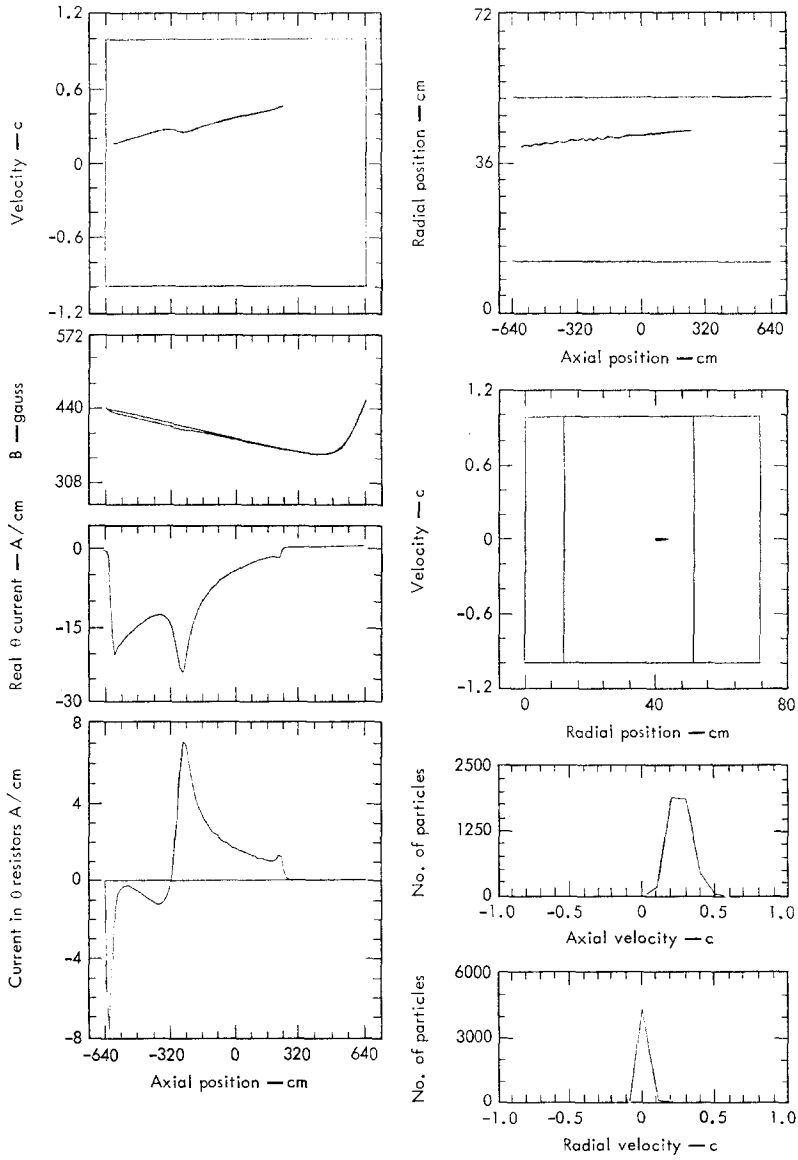

FIG. 4. State of the system at 100 nsec: (a) plot at the particle positions in $Z - V_z$ phase space; (b) plot of B_z vs Z; (c) current distribution of the particles; (d) current distribution in the resistors; (e) plot of the particle position in configuration space; (f) plot of the particles in $R - V_R$ phase space; (g) Z velocity distribution; and (h) R velocity distribution.

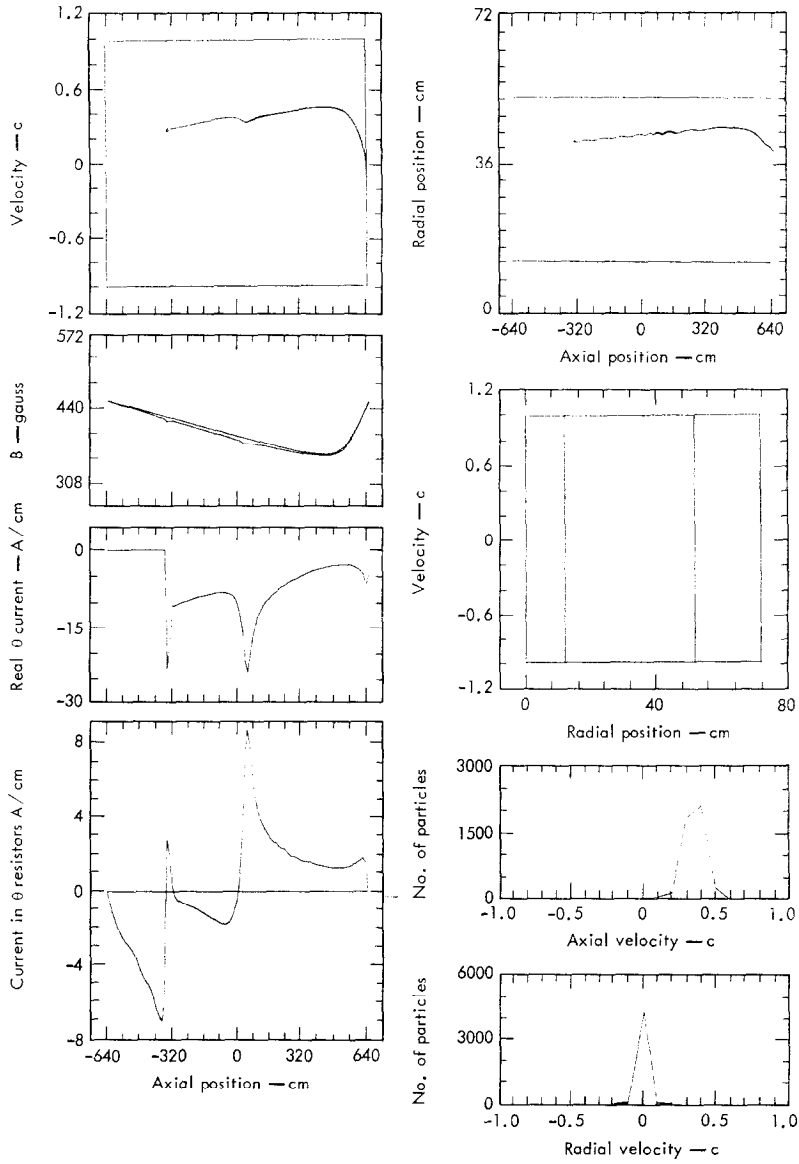

FIG. 5. State of the system at 148 nsec: (a) plot at the particle positions in $Z - V_z$ phase space; (b) plot of B_z vs Z; (c) current distribution of the particles; (d) current distribution in the resistors; (e) plot of the particle position in configuration space; (f) plot of the particles in $R - V_R$ phase space; (g) Z velocity distribution; and (h) R velocity distribution.

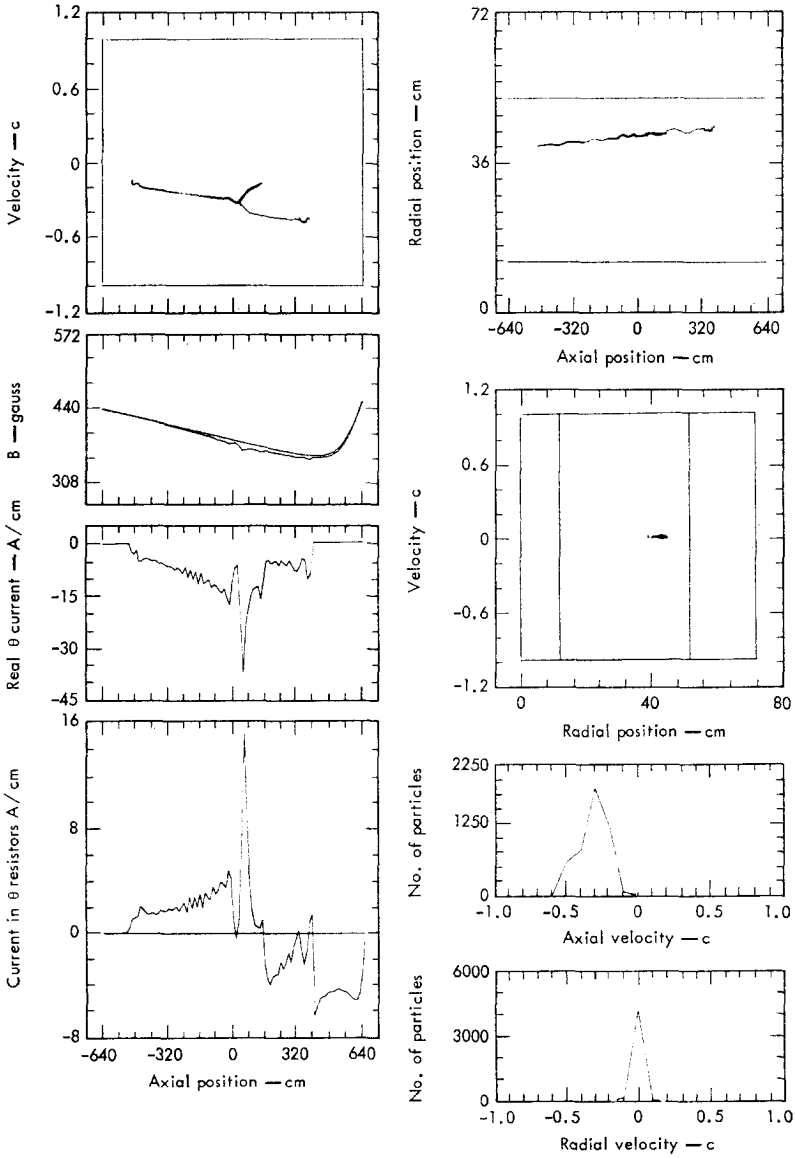

FIG. 6. State of the system at 268 nsec. (a) plot at the particle positions in $Z - V_z$ phase space; (b) plot of B_z vs Z; (c) current distribution of the particles; (d) current distribution in the resistors; (e) plot of the particle position in configuration space; (f) plot of the particles in $R - V_R$ phase space; (g) Z velocity distribution; and (h) R velocity distribution.

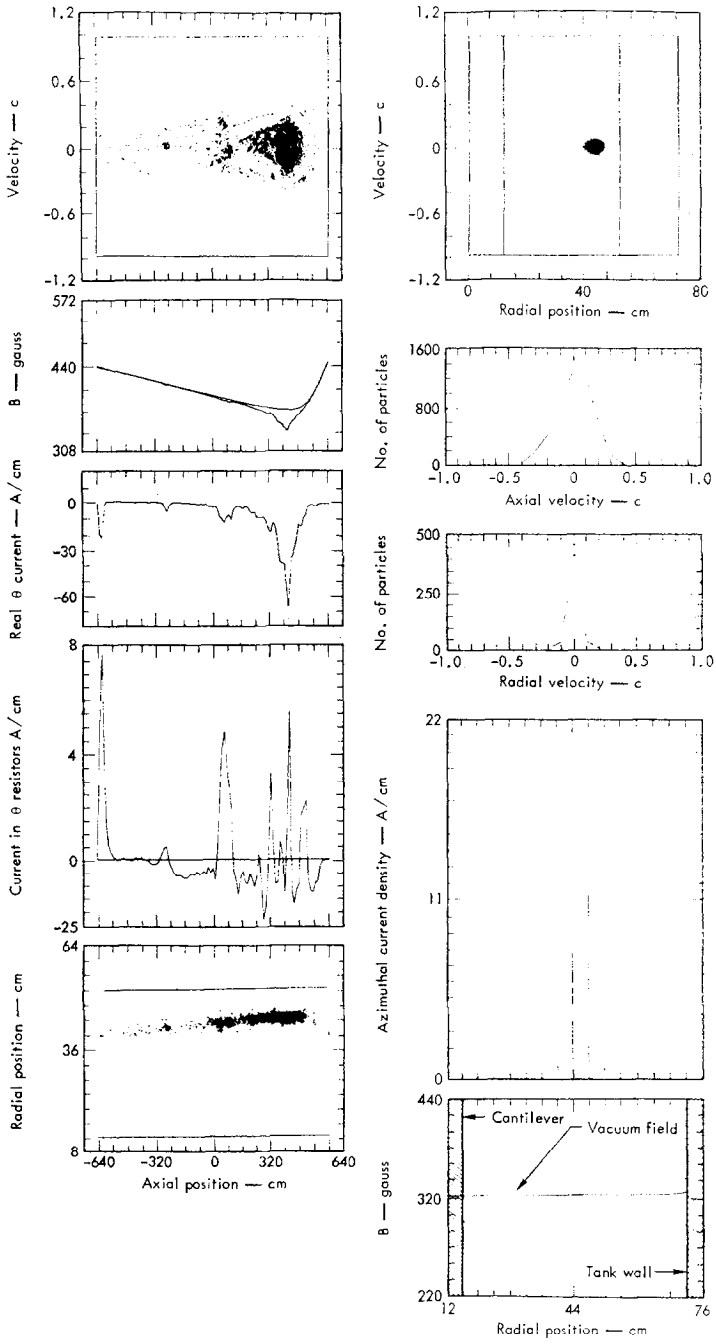

FIG. 7. State of the system at 1308 nsec: (b) plot at the particle positions in $Z - V_z$ phase space; (*b*) plot of B_z vs Z; (*c*) current distribution of the particles; (d) current distribution in the resistors; (e) plot of the particle position in configuration space; (f) plot of the particle position in $R - V_R$ phase space; (g) Z velocity distribution; (h) R velocity distribution; (i) radial variation of the current density at $Z = 10.8$ m; and (j) radial variation of B_z at $Z = 10.8$ m.

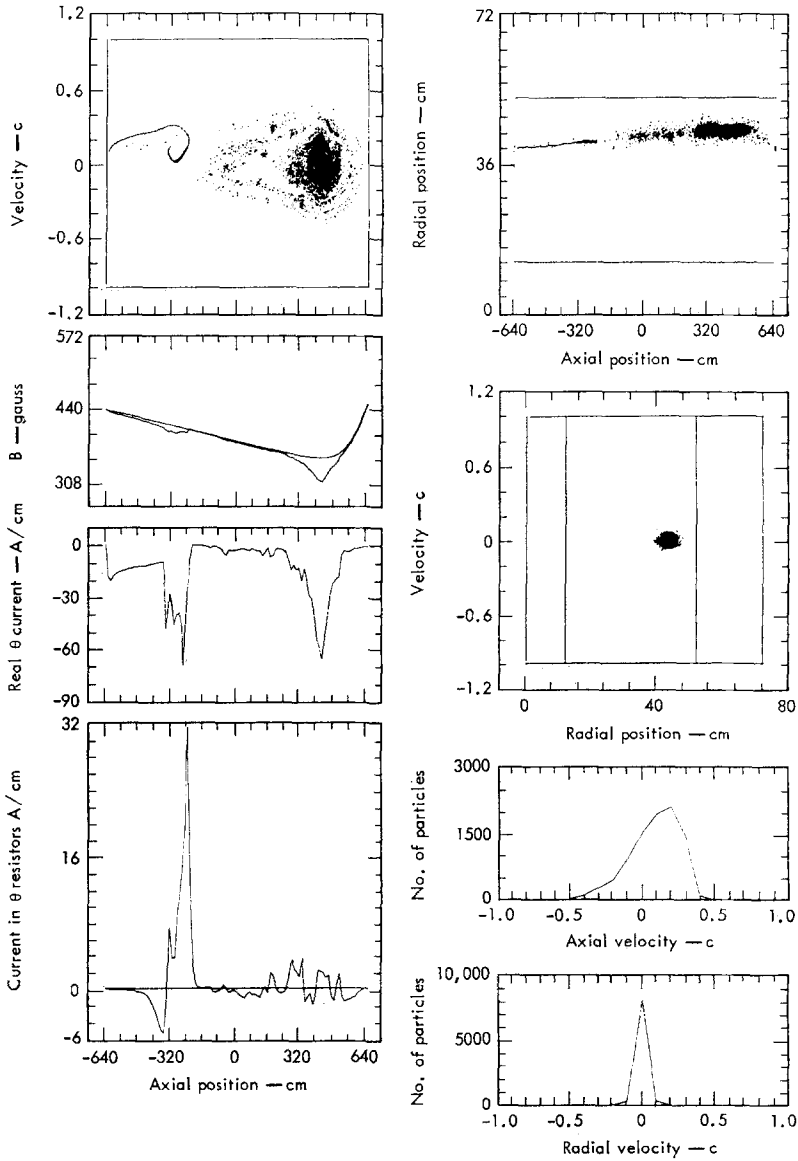

FIG. 8. State of the system at 1400 nsec: (a) plot at the particle positions in $Z - V_z$ phase space; (b) plot of B_z vs Z; (c) current distribution of the particles; (d) current distribution in the resistors; (e) plot of the particle position in configuration space; (f) Plot of the particle position in $R - V_R$ phase space; (g) Z velocity distribution; and (h) R velocity distribution.

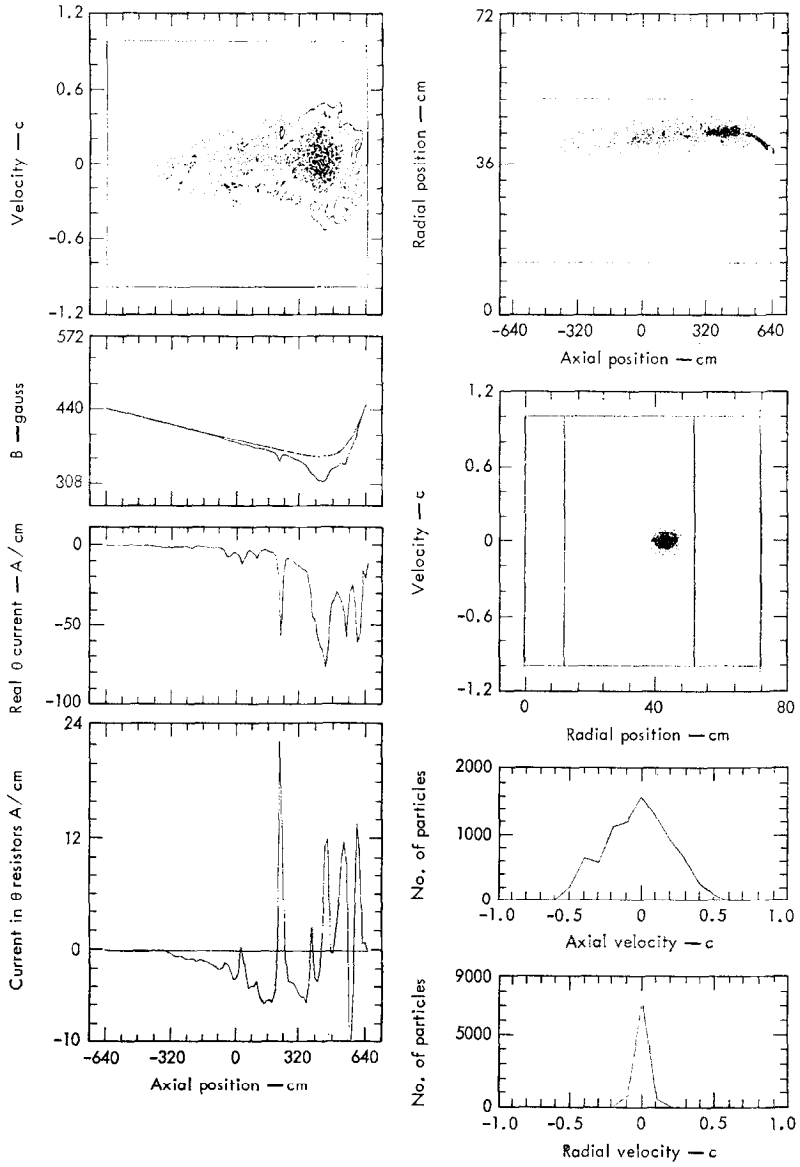

FIG. 9. State of the system at 1520 nsec: (a) plot at the particle positions in $Z - V_z$ phase space; (b) plot of B_z vs Z; (c) current distribution of the particles; (d) current distribution in the resistors; (e) plot of the particle position in configuration space; (f) plot of the particle position in $R - V_R$ phase space; (g) Z velocity distribution; and (h) R velocity distribution.

By $t = 2200$ nsec, the particles from the two pulses have become thoroughly intermixed (Figs. 10a, e, and f) and the system has reached steady state (Fig. 10g). From Figs. 10e and f we see that a few particles have collided with the resistors. With 18 239 amperes circulating in the system, the field at the bottom of the well has been reduced to 80% of its original value (Fig. 10j).

Injection of the third pulse began at $t = 2200$ nsec and ended at $t = 2300$ nsec (Fig. 11). The bulk of the third pulse reaches the end of the far mirror by $t = 2414$ nsec. As in the two previous pulses, some of the particles of the third pulse climb the far mirror and leave the system (Fig. 12a and e). In addition to this loss a steady drain of particles, primarily due to collisions with the resistors, is seen from then on. The system reaches steady state by $t = 2732$. By this time, 1115 particles have left the system. More than half of these did so by colliding with the resistors. We allowed the problem to run another 360 nsec before injecting the next pulse. During this time interval, an additional 494 particles have left the system. Most of these were wiped off by the resistors (Fig. 13). Comparison of Figs. 7i and 13i reveals that the E layer has virtually doubled in thickness. The 25 450 circulating amperes that are presently in the system yield 31% field reversal at the bottom of the well (Fig. 13j).

Injection of the fourth pulse began at $t = 3100$ nsec and ended at $t = 3200$ (Fig. 14). The particles from this pulse reach the far mirror by $t = 3308$ nsec (Fig. 15). Once again, some particles leave the system by climbing the far mirror (Figs. 15a and e). Steady state is again reached by $t = 3668$ nsec. Of the 18 000 particles that had been injected, 3753 were lost. During the last 567 nsec, from $t = 3100$ until $t = 3668$, 2144 had left the system. The vast majority of them were lost due to collision with the resistors. Once again we allowed the problem to run an additional 333 nsec before injecting the next pulse. During this time interval an additional 853 particles had been lost, primarily due to collision with the resistors (Figs. 16e and f). There are now 28 574 amperes circulating in the system. The field is now 68% of its vacuum value (Fig. 16j).

Injection of the fifth and final pulse began at $t = 4000$ (Fig. 16) and ended at $t = 4100$ (Fig. 17). The particles reach the far mirror by $t = 4200$ (Fig. 18). Steady state is again reached by $t = 4536$ nsec, 536 nsec after we started injecting the fifth pulse. During this time interval, 3156 particles were lost. We allowed the system to run an additional 184 nsec until $t = 4720$ (Fig. 19). During this time interval, an additional 571 particles have left the system. This brings the number of particles lost since we started injecting the fifth pulse to 3727. This is equivalent to 83% of the particles injected in the fifth pulse. The remaining particles yielded a circulating current of 30 222 A. This resulted in 35% field reversal (Fig. 19j).

In total, 8333 particles were lost (Fig. 20). This is almost equal to the number of particles injected in two pulses. The vast majority of these particles were lost

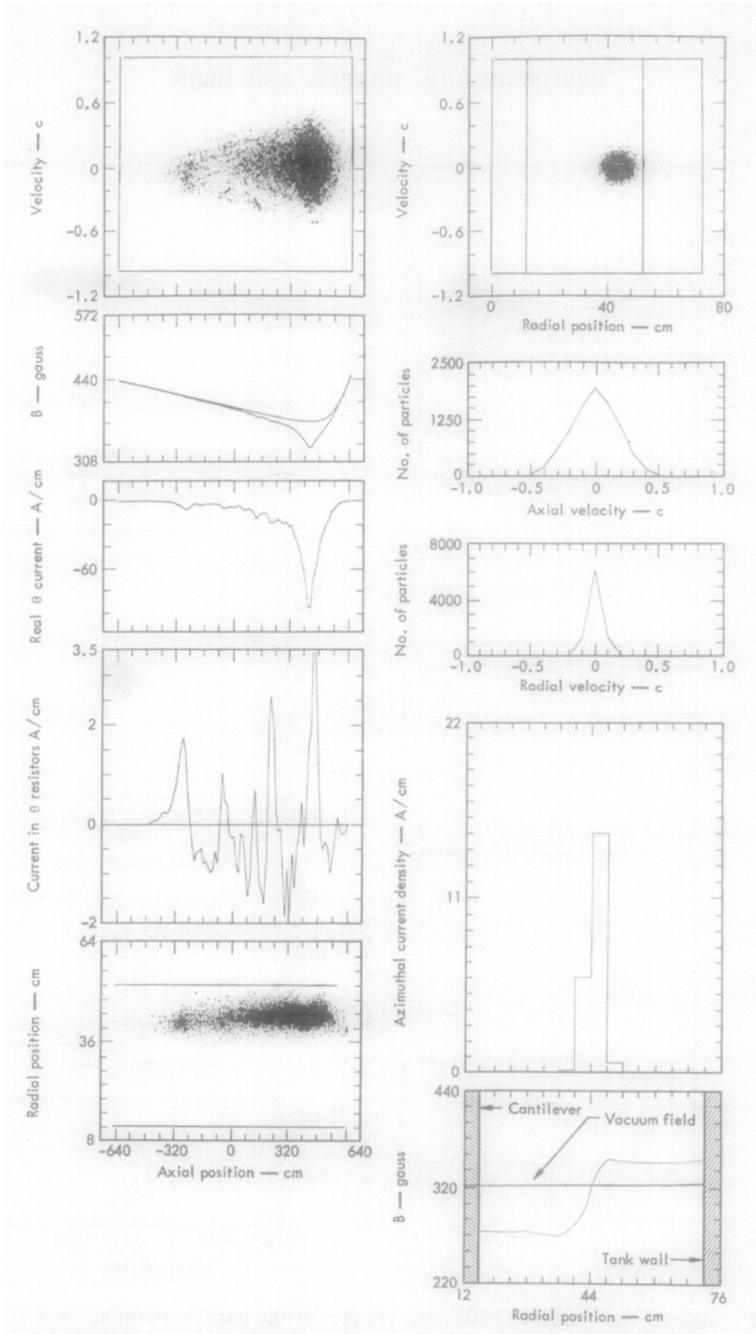

FIG. 10. State of the system at 2200 nsec: (a) plot at the particle positions in $Z - V_z$ phase space; (b) plot of B_z vs Z; (c) current distribution of the particles; (d) current distribution in the resistors; (e) plot of the particle position in configuration space; (f) plot of the particle position in $R - V_R$ phase space; (g) Z velocity distribution; (h) R velocity distribution; (i) radial variation of the current density at $Z = 10.8$ m; and (j) radial variation of B_z at $Z = 10.8$ m.

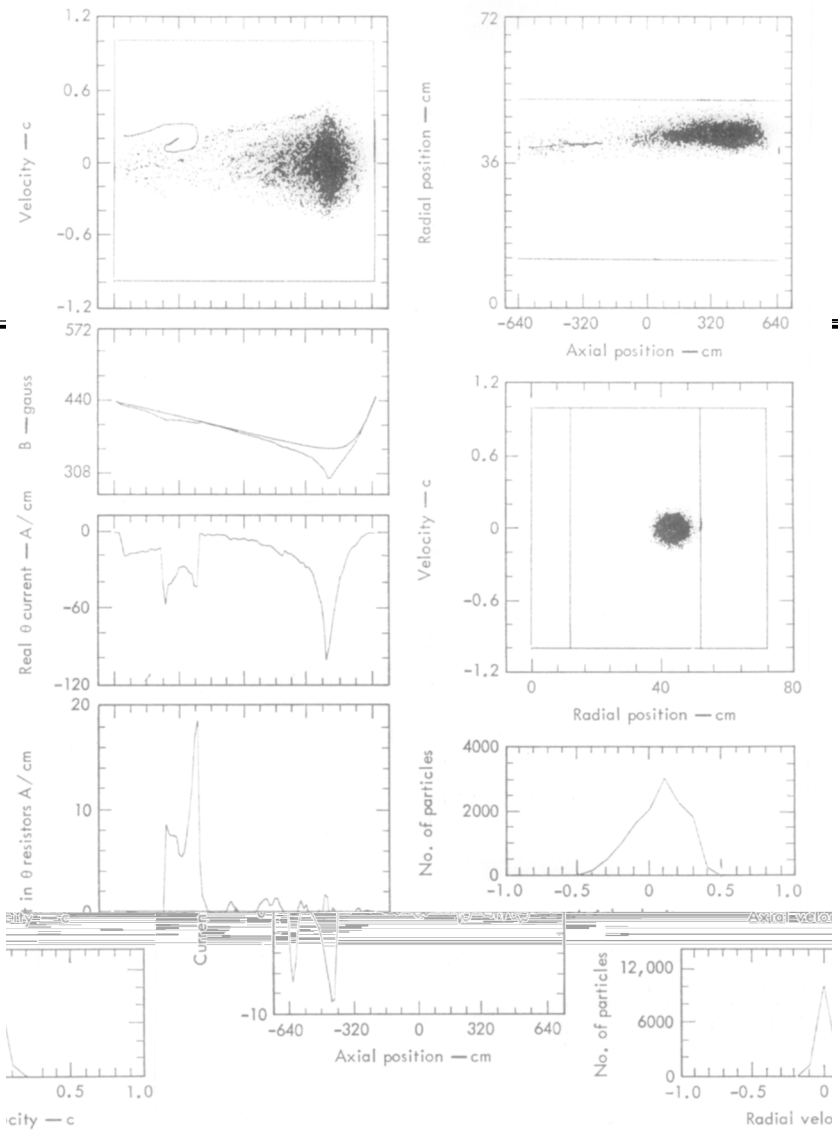

FIG. 11. State of the system at 2308 nsec. (a) plot at the particle positions in $Z - V_z$ phase space; (b) plot of B_z vs Z; (c) current distribution of the particles; (d) current distribution in the resistors; (e) plot of the particle position in configuration space; (f) plot of the particle position in $R - V_R$ phase space; (g) Z velocity distribution; and (h) R velocity distribution.

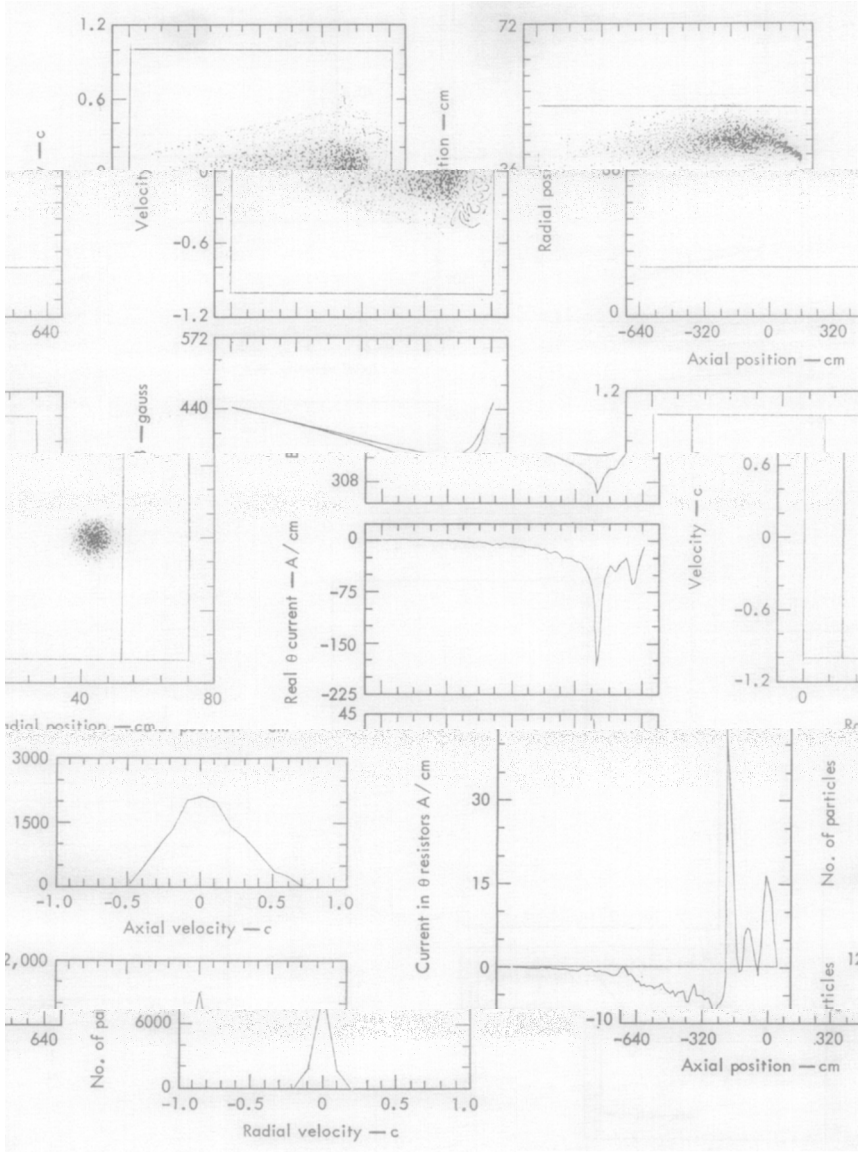

FIG. 12. State of the system at 2412 nsec. (a) plot at the particle positions in $Z - V_z$ phase space; (b) plot of B_z vs Z; (c) current distribution of the particles; (d) current distribution in the resistors; (e) plot of the particle position in configuration space; (f) plot of the particle position in $R - V_R$ phase space; (g) Z velocity distribution; and (h) R velocity distribution.

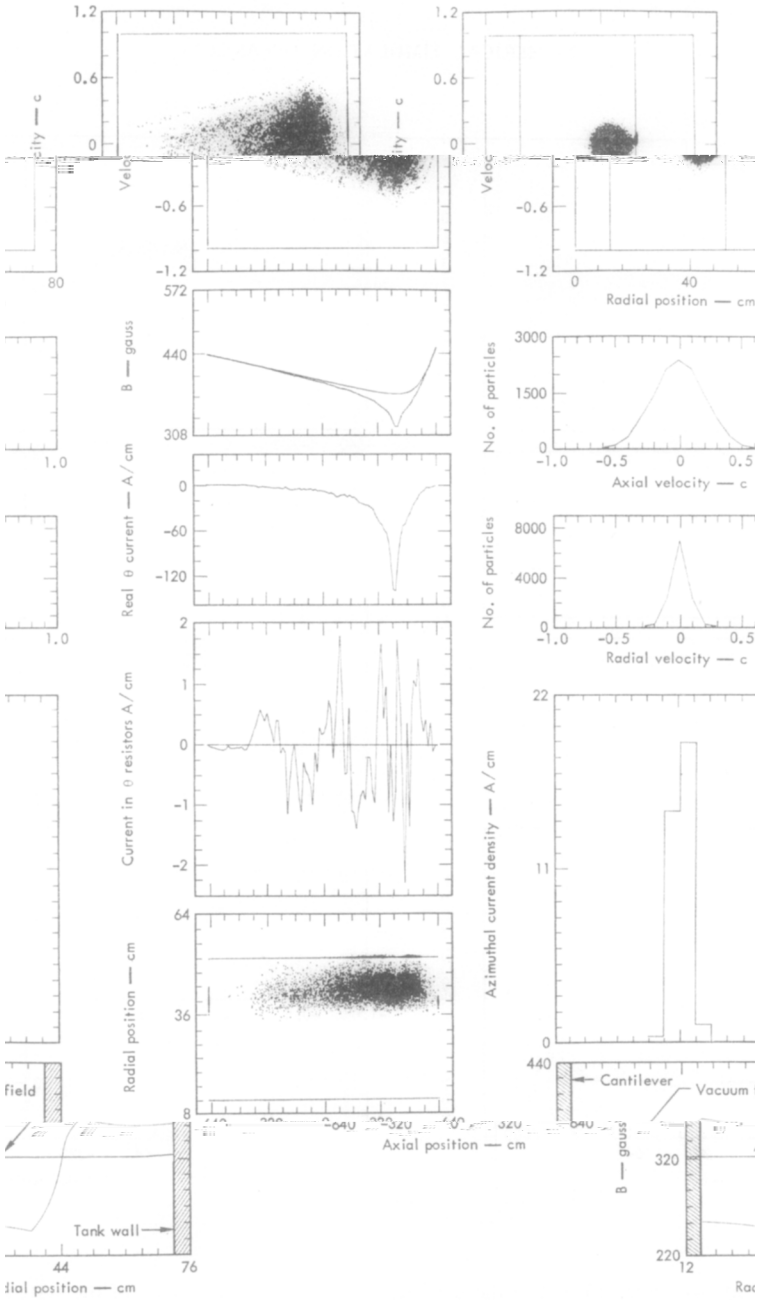

FIG. 13. State of the system at 3092 nsec: (a) plot at the particle positions in $Z - V_z$ phase space; (b) plot of B_z vs Z; (c) current distribution of the particles; (d) current distribution in the resistors; (e) plot of the particle position in configuration space; (f) plot of the particle position in $R - V_R$ phase space; (g) Z velocity distribution; (h) R velocity distribution; (i) radial variation of the current density at $Z = 10.8$ m; and (j) radial variation of B_z at $Z = 10.8$ m.

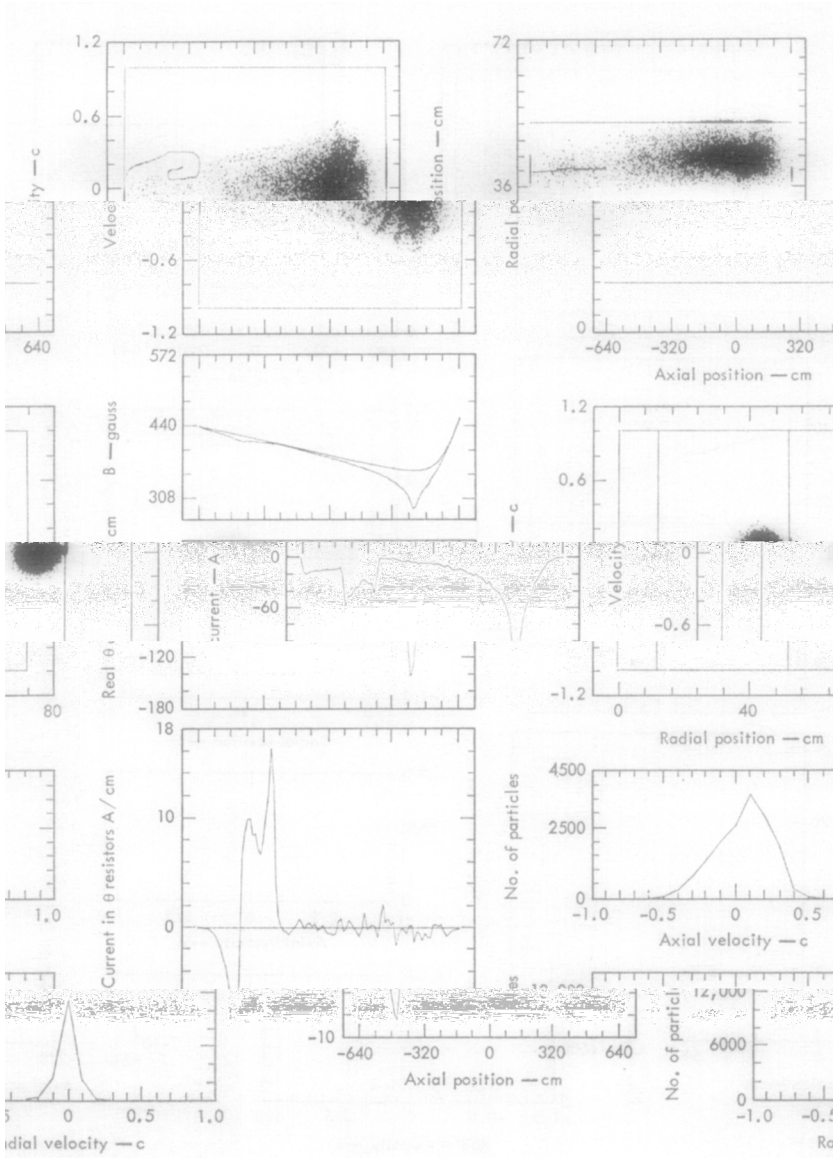

FIG. 14. State of the system at 3200 nsec: (a) plot at the particle positions in $Z - V_z$ phase space; (b) plot of B_z vs Z; (c) current distribution of the particles; (d) current distribution in the resistors; (e) plot of the particle position in configuration space; (f) plot of the particle position in $R - V_R$ phase space; (g) Z velocity distribution; and (h) R velocity distribution.

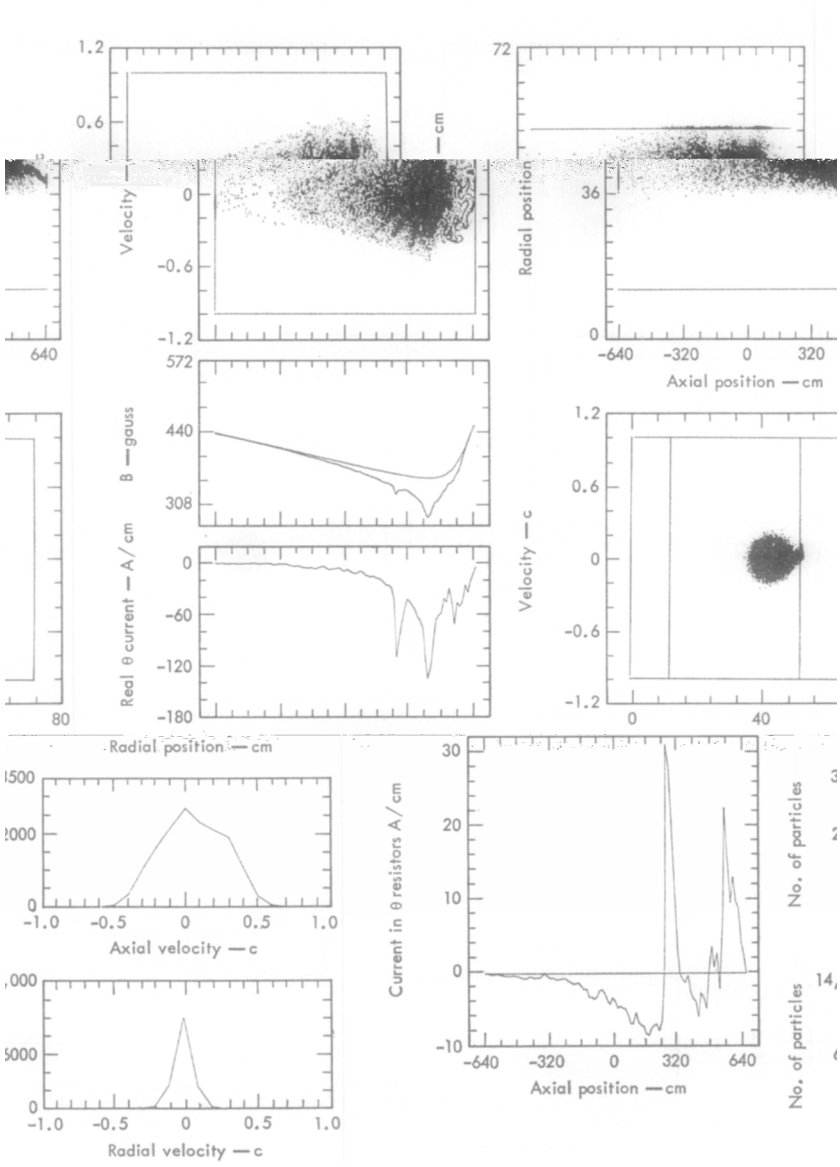

FIG. 15. State of the system at 3308 nsec. (a) plot at the particle positions in $Z - V_z$ phase space; (b) plot of B_z vs Z; (c) current distribution of the particles; (d) current distribution in the resistors; (e) plot of the particle position in configuration space; (f) plot of the particle position in $R - V_R$ phase space; (g) Z velocity distribution; and (h) R velocity distribution.

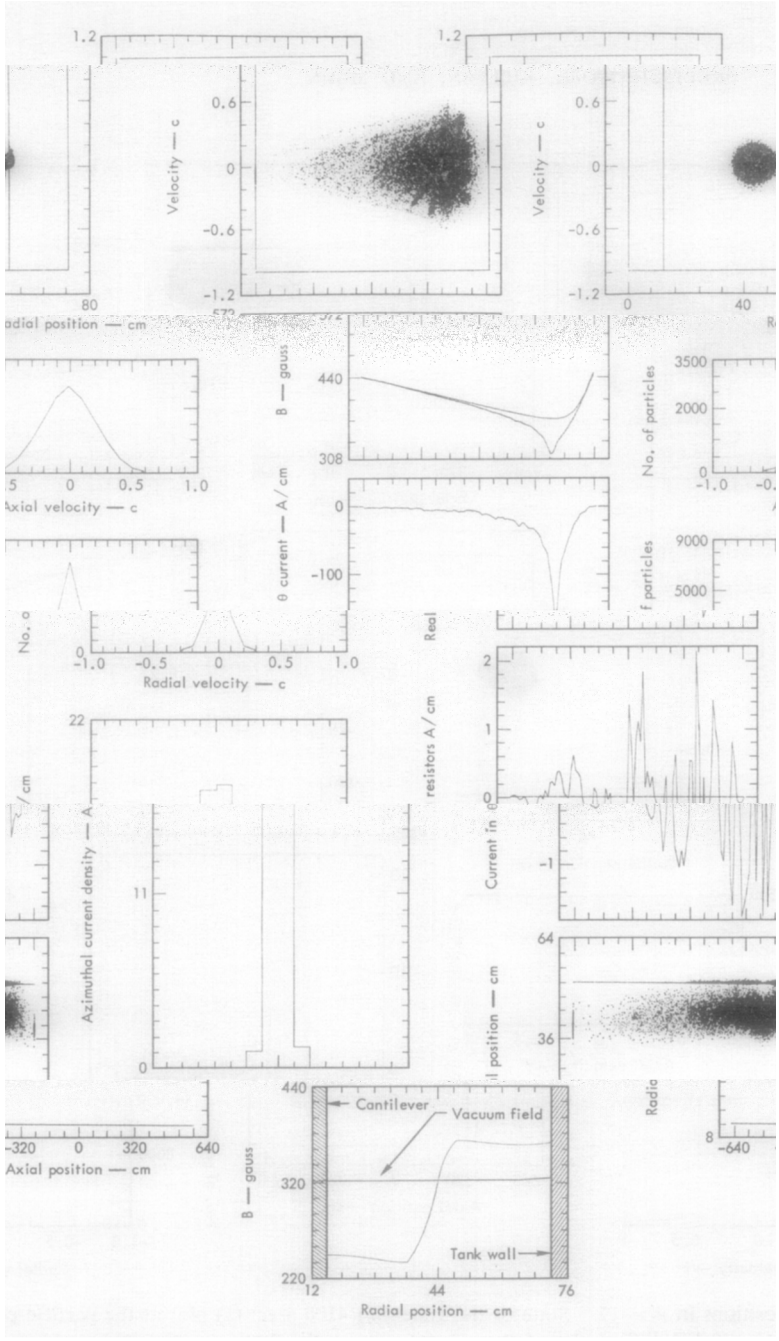

FIG. 16. State of the system at 4000 nsec: (a) plot at the particle positions in $Z - V_z$ phase space; (b) plot of B_z vs Z; (c) current distribution of the particles; (d) current distribution in the resistors; (e) plot of the particle position in configuration space; (f) plot of the particle position in $R - V_R$ phase space; (g) Z velocity distribution; (h) R velocity distribution; (i) radial variation of the current density at $Z = 10.8$ m; and (j) radial variation of B_z at $Z = 10.8$ m.

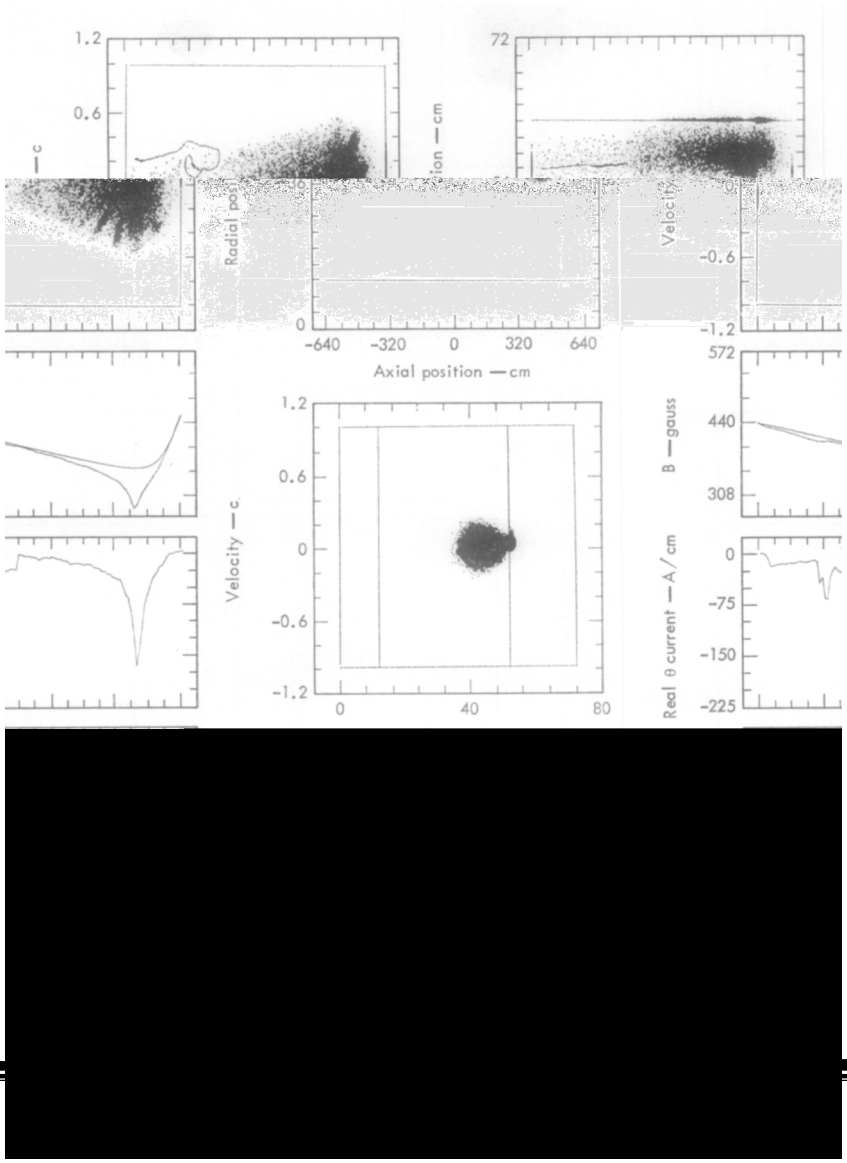

FIG. 17. State of the system at 4108 nsec: (a) plot at the particle positions in Z -- V_z phase space; (b) plot of B_z vs Z; (c) current distribution of the particles; (d) current distribution in the resistors; (e) plot of the particle position in configuration space; (f) plot of the particle position in R -- V_R phase space; (g) Z velocity distribution; and (h) R velocity distribution.

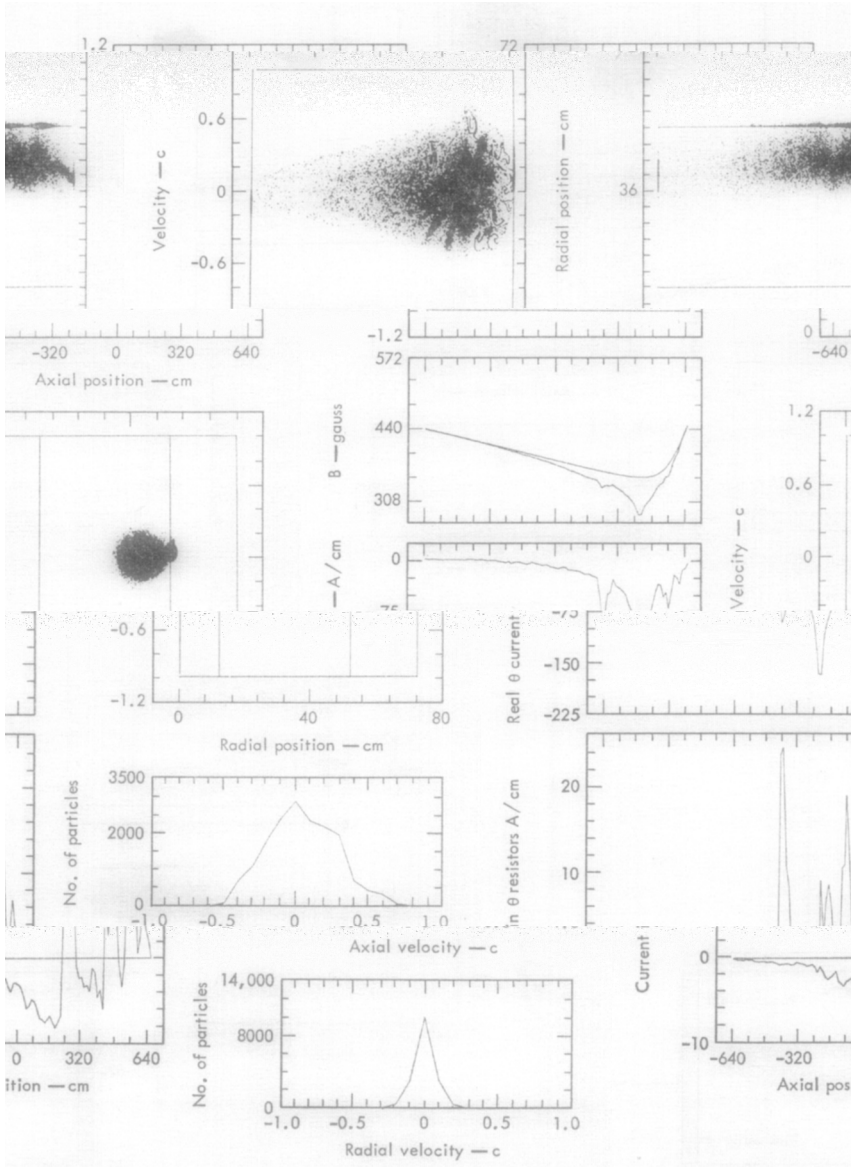

FIG. 18. State of the system at 4200 nsec: (a) plot at the particle positions in $Z - V_z$ phase space; (b) plot of B_z vs Z; (c) current distribution of the particles; (d) current distribution in the resistors; (e) plot of the particle position in configuration space; (f) plot of the particle position in $R - V_R$ phase space; (g) Z velocity distribution; and (h) R velocity distribution.

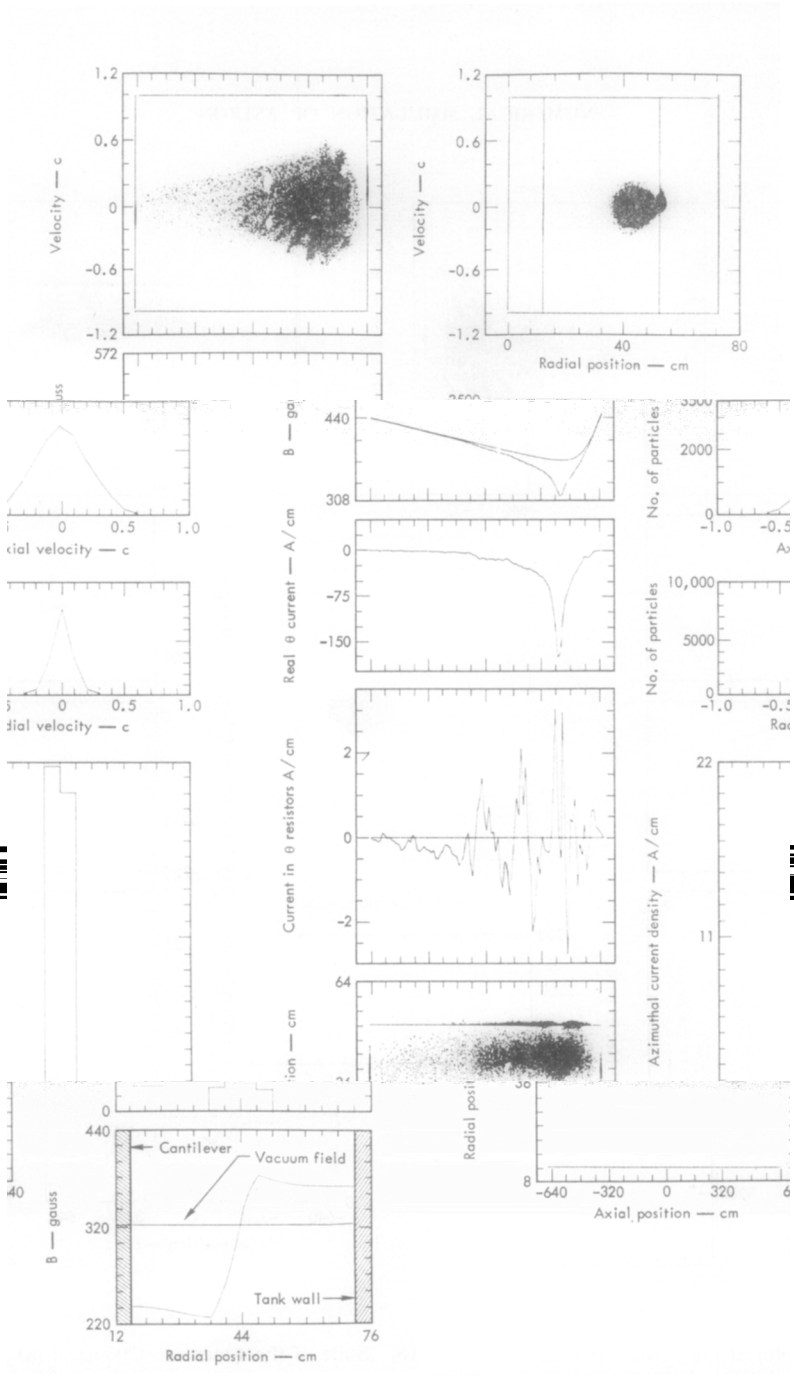

FIG. 19. State of the system at 4720 nsec: (a) plot at the particle positions in $Z - V_z$ phase space; (b) plot of B_z vs Z; (c) current distribution of the particles; (d) current distribution in the resistors; (e) plot of the particle position in configuration space; (f) plot of the particle position in $R - V_R$ phase space; (g) Z velocity distribution; (h) R velocity distribution; (i) radial variation of the current density at $Z = 10.8$ m; and (j) radial variation of B_z at $Z = 10.8$ m.

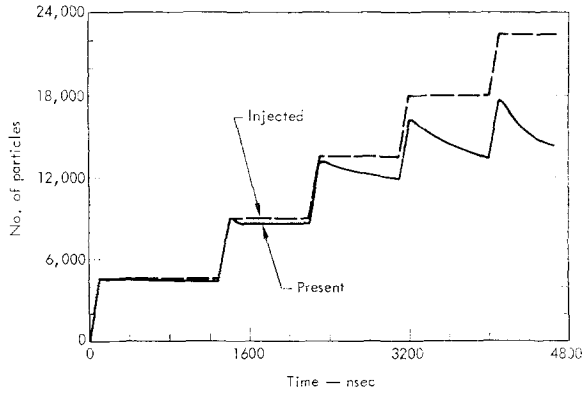

FIG. 20. Plot of number of particles vs time.

due to collisions with the resistors (Table I). During the first two pulses, particle loss is due primarily to particles climbing the far mirror. About 450 particles were lost in this way during these two pulses. However, during the last three pulses, particle loss is due primarily to collisions with the resistors.

Detailed comparison of these results with experiment is at present impossible because the astron group has not yet achieved a net injection current of 800 A. However, there are certain similarities between the higher current computations and the lower current observations. For instance, the time that it takes for an injected pulse to reach equilibrium is observed to be between 1 and 2 μ sec. The

TABLE I

Summary of Particle Losses

Pulse	Number particles injected	Number particles lost	Number particles lost at left-end boundary	Number particles lost at right-end boundary	Number particles lost at resistors	Number particles lost at cantilever
1	4500	2923	8	78	2762	0
2	4500	2742	148	341	2258	0
3	4500	1664	69	176	1419	0
4	4500	766	27	134	605	0
5	4500	236	43	177	16	0

computed time is about 1.4 μsec. It is also observed that the incoming pulse contains a rapidly moving leading edge of low amplitude followed by a slower moving clump at high amplitude. The same structure is seen in Fig. 4c.

In looking at the current density graphs, Figs. 8c, 10c, 13c, 16c, and 19c, it is evident that the width of half maximum tends to decrease with time. The most dramatic decrease occurs between the second and the third pulses. At $t = 2200$ nsec the width at half maximum was $\sim$92 cm, whereas at $t = 3100$ is was $\sim$69 cm. The same phenomenon has been observed experimentally.

The results described indicate that, in the regime for which the model is valid, the idea of building an E layer by injecting a succession of pulses is workable. However, the particles from only three pulses were trapped. The maximum current density achieved was 175 A/cm, resulting in $\sim$35 % field reversal. It appears that the physical configuration of the system will have to be modified if more particles are to be trapped. The obvious modification is to remove the resistors from the trap region. This region has an axial extent of about 3m, and its center is located about 11m from the injection point. Removal of the resistors from this region should still leave enough resistors in the ramp region to aid in trapping.

That a reversed field solution exists is not in doubt. Killeen [1, 4, 5] found such solutions with the Vlasov code LAYER. In Ref. [5] an example is given of a reversed field solution corresponding to 4000 A injection into a short magnetic mirror region of 180 cm length with injection at $r_0 = 30$ cm. The layer was completely neutralized and the field was obtained from a solution of the A_θ equation [Eq. (53)] only. The same problem was run with the present particle code, and at the end of 300-nsec injection, the amount of field reversal was the same as in the earlier problem. The Cornell group also obtained reversed field configurations experimentally with high-current injection [7].

The results to date are preliminary. Our aim in constructing this model was to make it into a flexible experimental tool. We have made provision for varying a large number of parameters. A large number of graphs are also provided. At present, we can vary the injection current, the pulse length, the number of pulses, and the number of particles used. The resistance and the position of the resistors and their configuration are variable. The applied magnetic field can be evaluated in two distinct ways, through the use of one of two analytical models or from a computer program called COILS, which calculates the field at any desired point in space due to a set of coils whose centers are on the axis. In addition, we can include an arbitrary toroidal field. All the above variables can, with a minor modification, be made time dependent.

In addition to astron, the model can be used to simulate many aspects of the Electron Ring Accelerator.

ACKNOWLEDGMENT

We wish to thank Drs. J. A. Byers, A. B. Langdon, and M. E. Rensink for many useful discussions and suggestions.

REFERENCES

1. J. KILLEEN, V. K. NEIL, AND W. HECKROTTE, *in* "Plasma Physics and Controlled Fusion Research," Vol. II, pp. 227–243, IAEA, Vienna, 1966.
2. C. H. WOODS, *Plasma Phys.* **12** (1970), 361.
3. M. BRETTSCHNEIDER AND P. B. WEISS, *Bull. Amer. Phys. Soc.* **13** (1968), 299, 1532.
4. J. KILLEEN AND S. L. ROMPEL, *J. Comput. Phys.* **1** (1966), 29.
5. J. A. BYERS AND J. KILLEEN, *in* "Methods in Computational Physics," Vol. 9, pp. 259–305, Academic Press, New York, 1970.
6. MIRIN, AND M. L. RENSINK, *in* "Plasma Physics and Controlled Fusion Research," Vol. I, pp. 137–167, IAEA, Vienna, 1971.
7. M. L. ANDREWS, H. DAVITIAN, H. H. FLEISCHMANN, R. E. KRIBEL, B. R. KUSSE, J. A. NATION, R. LEE, R. V. LOVELACE, AND R. N. SUDAN, *in* "Plasma Physics and Controlled Fusion Research," Vol. I, pp. 169–180, IAEA, Vienna, 1971.